BROADBAND MICROWAVE SURFACE IMPEDANCE MEASUREMENTS ON $La_{0.8}Sr_{0.2}MnO_3$

by

Marc Scheffler

Thesis submitted to the Faculty of the Graduate School of the
University of Maryland, College Park in partial fulfillment
of the requirements for the degree of
Master of Science
1998

UNIVERSITY OF MARYLAND

DEPARTMENT OF PHYSICS

COLLEGE PARK, MARYLAND 20742

ABSTRACT

Title of Thesis:	BROADBAND MICROWAVE SURFACE IMPEDANCE MEASUREMENTS ON $La_{0.8}Sr_{0.2}MnO_3$
Degree candidate:	Marc Scheffler
Degree and year:	Master of Science, 1998
Thesis directed by:	Professor Steven M. Anlage
	Department of Physics

The complex microwave surface impedance offers the opportunity to observe the characteristic high frequency response of samples. In the case of $La_{0.8}Sr_{0.2}MnO_3$, a colossal magnetoresistive material, in the temperature range around the phase transition from ferromagnet to paramagnet both the magnetic and the electrical behavior can be studied.

Our experiment employs the Corbino geometry to measure the surface impedance in the complete frequency range from 45 MHz to 20 GHz, which distinguishes it from resonant microwave experiments. The surface impedance of a $La_{0.8}Sr_{0.2}MnO_3$ single crystal has been measured as a function of frequency, temperature and applied magnetic field. As typical for ferromagnets at microwave frequencies, $La_{0.8}Sr_{0.2}MnO_3$ exhibits the effects of ferromagnetic resonance and antiresonance, characteristic maxima and minima in the surface resistance at particular frequencies, depending on magnetization and external magnetic field.

Resonance and antiresonance are observed not only in the dependence of the applied magnetic field, as it is usual for resonant techniques, but also in the frequency dependence. From the ferromagnetic antiresonance in the absence of an external field, the spontaneous magnetization is deduced and its temperature dependence presented. To explain the experimental results an established model for the dynamic susceptibility is extended to apply to the specifics of our measurements, especially the case of low applied magnetic fields and non uniformity of magnetic field and magnetization.

BROADBAND MICROWAVE SURFACE IMPEDANCE MEASUREMENTS ON $La_{0.8}Sr_{0.2}MnO_3$

by

Marc Scheffler

Thesis submitted to the Faculty of the Graduate School of the
University of Maryland, College Park in partial fulfillment
of the requirements for the degree of
Master of Science
1998

Advisory Commitee:

Professor Steven M. Anlage, Chair
Professor Richard L. Greene
Professor Ramamoorthy Ramesh

DEDICATION

To my parents

ACKNOWLEDGMENTS

When I came to the University of Maryland in August 1997, I planned to have a two semester long experience of the United States in general and of the American university system in particular, but I did not expect to earn an academic degree. Earlier this year I decided to head for a Master of Science degree, but although I wanted to write a thesis, I did not expect at all the deep involvement in current research that it turned out to be.

I was extremely fortunate to work in the high frequency group directed by Professor Steven Anlage. He offered me a project that turned out to be not only suitable for a Master's thesis, but also to be real research at its best, with unexpected results and complete shifts of the focus of interest. Furthermore he is an advisor who keeps close contact to the members of his group, which makes it possible for us to benefit directly from his extensive knowledge in experimental physics.

The research described here would not have been possible without Andrew Schwartz. There was almost no day that I did not seek and find his help, first to keep the experimental setup running, later in planning new experiments and understanding the data.

Furthermore I want to thank the other members of the high frequency group with whom I shared the lab, in particular Johan Feenstra, Lucia Mercaldo, David Steinhauer and Vladimir Talanov. I also want to thank Dave particularly for his support in using the scanning near-field microwave microscope.

In the Center for Superconductivity Research I want to thank Professor Greene and Professor Ramesh for being members of my thesis committee. Also I want to thank the Center staff for help with my administrative problems.

Furthermore I want to thank Patrick Fournier for conducting SQUID magnetization measurements on our sample.

In the physics department I also want to thank those people who helped me overcome the administrative obstacles on my way to the Master's Degree. In particular I want to thank Professor Richard Ellis for his support in having the possibility of a degree in my mind and helping me fulfill the requirements.

I am also indebted to all those who made my stay in the USA possible at all. The fact that I came to Maryland would not have been possible without the Fulbright Commission. Similarly I thank the German National Scholarship Foundation for their support. I also want to thank the members of the studies abroad office at my university in Braunschweig for their innumerable help.

Finally I want to thank my family for their support. My parents did not only support my idea to study in the USA from the beginning, but they also accepted my decision to stay longer than originally planned, although I probably could have helped my family better if I had gone back to Germany. I also want to thank my grandparents for their support and my sister for her strong encouragement to head for a master's degree.

TABLE OF CONTENTS

LIST OF FIGURES

1 Introduction

1.1 Colossal Magnetoresistive Materials and their Microwave Surface Impedance

Since the discovery of colossal magnetoresistance (CMR), a drop of the dc resistance by orders of magnitude under application of a magnetic field, in manganites [1, 2] this class of materials has been the focus of much scientific research. While applications of these remarkable materials seem to be in close reach, the theoretical understanding of the underlying mechanisms for their behavior is still not complete, although theories like double-exchange are considered to be promising starting points. Therefore any experiment that may reveal new fundamental characteristics of these compounds may help to come closer to this goal.

CMR materials show, among other features, temperature dependent electrical and magnetic characteristics, connected to a transition from a ferromagnetic to a paramagnetic state, and to a transition from a metal-like electrical conductivity to a semiconductor-like state in the same temperature range. Since the microwave surface impedance Z_s depends on the electrical as well as on the magnetic properties of the material under study, microwave measurements are one possible access to their magnetic behavior. This is especially true for the effects of ferromagnetic resonance and antiresonance, two characteristic phenomena at microwave frequencies.

1.2 Microwave Surface Impedance Measurements

Since the surface impedance is a physical quantity that offers experimental access to information sought after in many different fields of solid state physics, different approaches to measure Z_s have been developed. Many measurements of Z_s employ resonant techniques, e.g. resonant cavities. Those experiments offer

a high sensitivity to measure Z_s, but by the nature of the resonant setup, their observations are limited to certain, discrete frequencies. Broadband experiments on the other hand allow for the measurement of the frequency dependence of Z_s, but their sensitivity is in general lower than those of resonant experiments. But the CMR materials are so lossy that little is gained from resonant experiments, hence broadband experiments are more suitable and reveal more information.

1.3 Ferromagnetic Resonance and Antiresonance

One strong feature in microwave surface impedance measurements of ferromagnetic materials is the ferromagnetic resonance (FMR). This effect, a peak of the surface resistance R_s, occurs if the sample is exposed to a microwave signal of the same frequency as the eigenfrequency of the precession of its magnetization around the magnetic field. Therefore the resonance frequency depends on the magnetization of the sample and the applied external magnetic field. FMR has been studied in a wide range of magnetic materials, among them CMR compounds in the form of thin films and single crystals, and has proven to be a powerful tool to investigate the magnetic behavior in general.

A closely related effect is the ferromagnetic antiresonance (FMAR). This causes a minimum in R_s and again occurs at specific frequencies, magnetizations and external fields. Both FMR and FMAR are strong features that can be easily observed in the interesting temperature region of the magnetic phase transition and therefore reveal information about the magnetic behavior in this regime. Furthermore FMAR offers a way to determine the magnetization of the sample with zero applied external field, a truly spontaneous magnetization.

2 Corbino Experiment

2.1 Experimental Setup

2.1.1 General Setup of the Experiment

The goal of our experiment is to measure the complex microwave surface impedance Z_s of the sample as a function of frequency as well as its dependence on temperature and external magnetic fields. Measuring the complete frequency dependence requires a broadband technique, as opposed to resonance setups. Resonance experiments usually allow for a very high precision in the determination of the surface impedance, but by the nature of their geometry they are restricted to the few resonant frequencies of their apparatus.

The idea of how to extract the complex surface impedance with our experiment is to measure the complex reflection coefficient S_{11} of the sample, a quantity directly related to Z_s. Therefore a microwave signal is generated and sent to the sample, which terminates a coaxial transmission line. The reflected wave is then detected and S_{11} is calculated as the complex ratio of the voltages of the detected and emitted signals.

The measurements were performed with an apparatus that was originally devised to observe vortex dynamics and fluctuation conductivity in high temperature superconductors [3, 4, 5]. Since the current experiments have a different goal, the setup and the operating procedure were changed slightly according to the new requirements, although the general idea of the experiment has not changed.

A schematic diagram of the general experimental setup is shown in figure (1). Its basis is a vector network analyzer (NWA). The microwave signal is generated by an HP 83651A series synthesized sweeper and sent through the NWA test set into a coaxial transmission line. This leads into a continuous flow cryostat and ends in a modified microwave connector. The sample is pressed against this con-

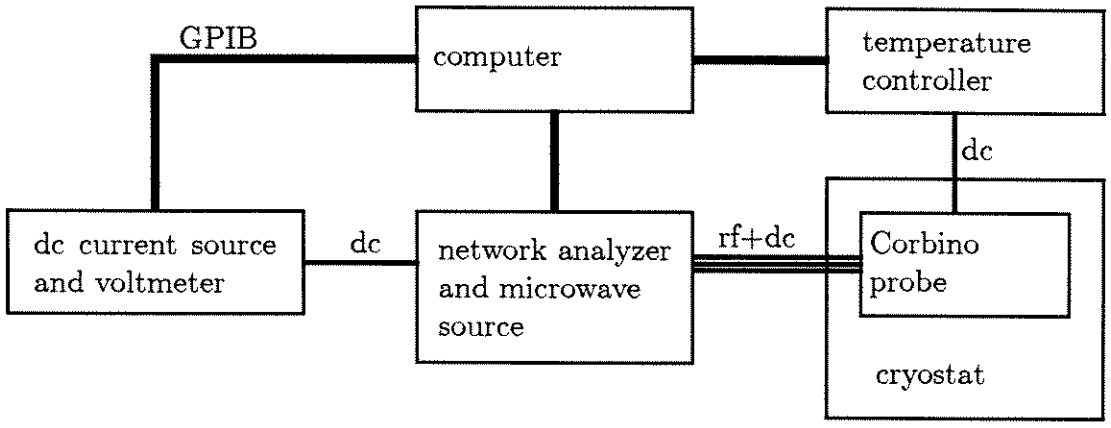

Figure 1: Schematic diagram of the general experimental setup

nector probe and thus reflects the microwave signal. The reflected signal passes through the coaxial cable again and is then compared with the outgoing wave by an HP 8510C Network Analyzer. The frequency range in which this apparatus can operate is 45 MHz to 50 GHz. Unfortunately the maximal microwave power supplied by the source decreases with increasing frequency. To ensure a constant output power of -22 dBm the measurements described here never exceeded 45 GHz.

In addition to the measurements at microwave frequencies it is possible to simultaneously determine the dc resistance of the sample in a two-point geometry. A dc current is sent through the coaxial transmission line and the voltage drop can be measured. The absolute value of the measured resistance includes the wires and the contact resistance in addition to the resistance of the sample, but relative changes can easily be determined by this method.

The continuous flow cryostat is cooled by liquid nitrogen, the temperature is stabilized by a temperature controller that uses a heater inside the cryostat. During the measurements the temperature was held constant within a few millikelvin. The whole experiment, that is the temperature controller, the network analyzer, the dc current source and the dc voltmeter, is controlled and the data are collected by a

computer. For the measurement itself and the data correction described in a later section a set of specifically developed LabView programs is used.

2.1.2 Corbino Probe

The Corbino probe itself and the way the sample is mounted in it is shown in figure (2). The core of the experiment, the Corbino probe, is a modified commercial

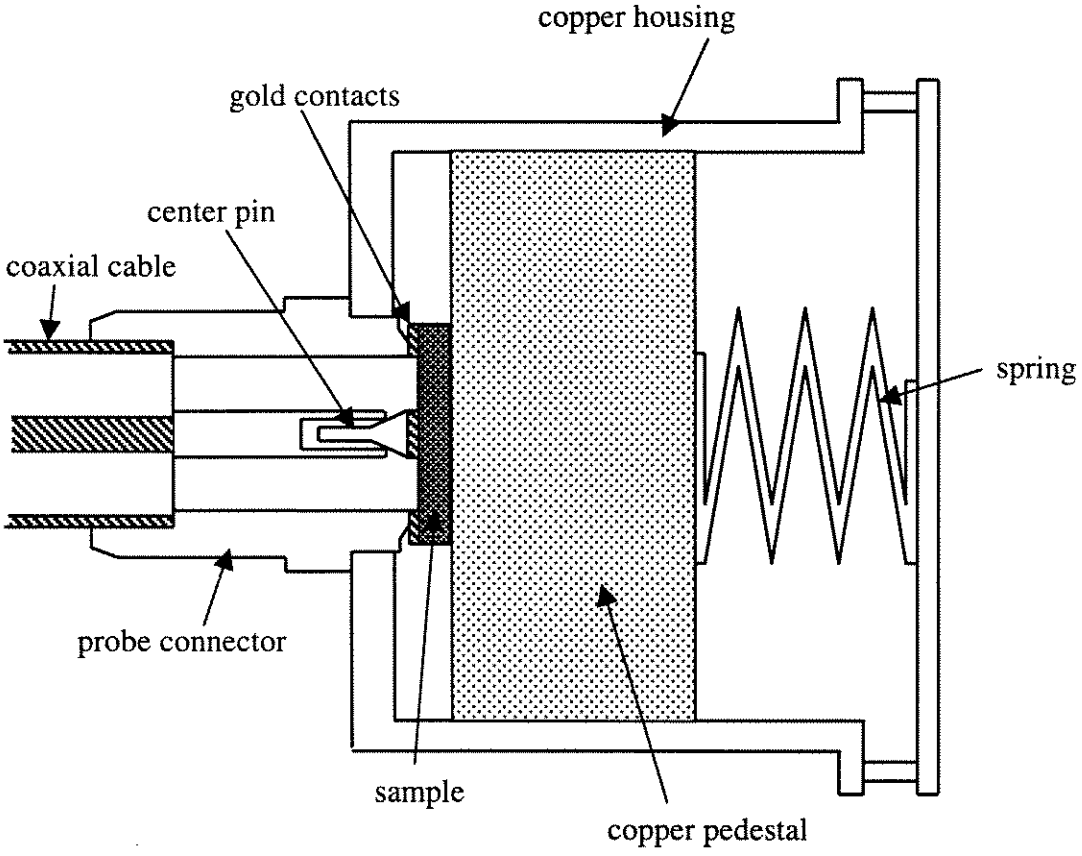

Figure 2: Schematic view of the Corbino probe (not to scale)

Wiltron V101F microwave connector for the 0.086-inch outer diameter coaxial transmission line. This makes it possible to use the probe as a usual microwave connector, which is important since the calibration standards used during the room temperature calibration are commercial standards. But due to the modifications of

the probe a flat disk-shaped sample can also be used to terminate the microwave transmission line. To do so the sample is supported by a copper pedestal and pressed against the probe connector by a spring. The copper pedestal as well as the probe are arranged inside a copper housing. The connector probe has a hollow center conductor that is slightly shorter than the outer conductor of the connector. To achieve electrical contact between the center conductor and the sample, a small pin is inserted into the center conductor of the connector and spring loaded.

To decrease the contact resistance between the sample and the connector, gold contacts are deposited on the sample. The gold pads are approximately 500 Å thick and are deposited by electron beam evaporation using shadow masks. The gold covers everything except a ring of the surface of the sample. This ring corresponds to the dielectric spacing of the connector and forms the Corbino disk, which is the region of the sample that actually contributes to the measurements. The outer conductor of the connector and the center pin inserted into the inner conductor touch the gold contacts.

2.1.3 Magnetic Field

Some of the experiments described below require the presence of a static magnetic field. There are two different ways in which the fields are realized, depending on the orientation of the field with respect to the sample disk. To obtain a magnetic field perpendicular to the disk, a permanent magnet is fixed onto the copper pedestal and the sample is positioned right on top of that magnet. The pedestal with magnet and sample is then inserted into the copper barrel as usual. The field strength is thus determined only by the strength of the magnet and cannot be changed except by changing the magnet.

A magnetic field parallel to the sample disk can be created by two permanent magnets. They are positioned in attractive orientation on opposite sides of

the sample, outside the cryostat. The distance between the two magnets can be changed continuously and by this means the strength of the magnetic field can be varied. The accessible range is between 0.19 T and 0.014 T.

2.1.4 Obtaining the Surface Impedance

The quantity measured by the network analyzer is the complex reflection coefficient S_{11}. To exclude influences other than those caused by the sample, a careful calibration is necessary. The calibration procedure is described in detail in the next section. Thus the reflection coefficient of the sample is obtained. But the reflection coefficient is directly related to the load impedance Z_L of the sample by the formula

$$S_{11} = \frac{Z_L - Z_0}{Z_L + Z_0} \quad \Leftrightarrow \quad Z_L = Z_0 \frac{1 + S_{11}}{1 - S_{11}}$$

where Z_0 is the impedance of the transmission line, $(50+i0)\,\Omega$. The load impedance Z_L and the surface impedance Z_s are related by a proportionality factor:

$$Z_s = \frac{2\pi}{\ln(\frac{b}{a})} Z_L$$

Here a and b are the inner and outer diameters of the connector, respectively. Thus the surface impedance of the sample can be extracted from its reflection coefficient S_{11}.

2.2 Calibration

2.2.1 Room Temperature Calibration

The primary quantity received by our experiment is the complex reflection coefficient S_{11} as measured by the vector network analyzer (NWA). This quantity is the voltage ratio of the wave detected by the NWA divided by the wave it emitted. But S_{11} reflects all effects on the electromagnetic wave from its departure from the NWA until it finally returns to it and also effects within the NWA. Thus not only

the sample of interest influences S_{11}, but also the whole transmission line between the NWA and the sample. Actually, the sample will give only a small contribution to S_{11} compared to the other effects. To extract the influence of the sample from this overall S_{11}, a calibration is necessary which will leave the sample as the only source of the reflection coefficient.

There are three general possible errors terms that affect S_{11}-measurements and which may be described by appropriate error coefficients: directivity, source match and reflection tracking [6]. The directivity E_D describes the leakage of a part of the signal from the source directly to the microwave detector due to limitations of the directional couplers inside the NWA. The source match E_S is due to partial rereflection of the signal coming from the sample back to it (caused by impedance mismatch inside the NWA) and reflection tracking E_R is the change (attenuation and phase offset) of the signal in the transmission line. Because of these three error terms, which are frequency dependent, the reflection coefficient S_{11m} measured by the NWA will not be the actual reflection coefficient S_{11a} of the sample under study, but instead

$$S_{11m} = E_D + \frac{E_R S_{11a}}{1 - E_S S_{11a}}$$

This means, that if the error coefficients are known, the actual reflection coefficient S_{11a} can be reconstructed from the measured reflection coefficient S_{11m} as

$$S_{11a} = \frac{S_{11m} - E_D}{E_R + E_S(S_{11m} - E_D)}$$

But to proceed in this way, it is necessary to know the three error coefficients. They may be obtained by measuring the reflection coefficients S_{11m} of three known devices with reflection coefficients S_{11}^{std}. Thus one has three relations for three unknowns and the error coefficients may be extracted.

The calibration procedure is as follows. The three standard devices are a perfect short, a perfect open, and a perfect load. The reflection coefficients of these devices are measured as a function of frequency over the frequency range of

interest and the error coefficients are calculated by the NWA. Then this calibration is automatically applied by the NWA to correct for the three error terms during subsequent measurements.

This calibration allows the reflection coefficient of the sample at the end of the transmission line to be extracted, as if it was measured directly inside the NWA without any error contributions. ("The plane of measurement was shifted from the NWA to the end of the probe connector.")

If this calibration is to be applied to the measurements, the sample has to be placed exactly where the calibration standards were attached. Therefore our probe is a modified standard Wiltron 1.85 mm microwave connector which allows the standard devices to be attached in the same way as at a usual connector, but also allows our sample to be pressed against it, creating the Corbino disk, and to measure its reflection coefficient.

2.2.2 Temperature Dependent Calibration

The calibration described above has to be performed at room temperature and is strictly valid only for that temperature, because the error terms are not necessarily temperature independent. Since our actual measurements cover a temperature range from 250 K to 325 K the room temperature calibration has to be modified to apply to all our measurements.

Of the three error terms described above the directivity and the source match are caused by imperfections inside the NWA and therefore can be assumed to be independent of temperature changes inside the cryostat. But the reflection tracking is caused by the whole transmission line. Since the probe connector and part of the coaxial cable are inside the cryostat, their temperature will change during the measurements and therefore the reflection tracking will also change.

Thus the calibration will not be valid at temperatures other than room

temperature. To account for this a further calibration procedure is conducted. A bulk piece of copper, in fact the copper pedestal which supports the sample during measurements, is measured as a further calibration standard. It is measured in the same way (at the same temperatures and frequencies) as is the sample. Then one assumes that this copper block acts as if it was a perfect short at all temperatures and therefore has a known reflection coefficient $S_{11}^{Cu} = -1 + i0$ as a standard to obtain the one temperature dependent error term E_R. Thus the error coefficients are determined for all frequencies and temperatures of interest and the reflection coefficient of the sample can be deduced from the measured reflection coefficient.

The use of the copper block as a calibration standard also solves another problem. The calibration assumes that the standards are attached exactly at the same place as is the sample to be measured. But the room temperature standards have connectors that mate to the probe connector, whereas the sample is a flat piece of material. To have reproducible contact between sample and probe it is necessary to insert a small pin into the center conductor of the probe connector, which gives the electrical contact (see figure 2). But since this pin was not present during the room temperature calibration, it will introduce new contributions to the reflection tracking that will not be accounted for by the room temperature calibration. However, the copper block as a standard is also measured with this pin. Thus this new error will also be removed by the calibration using the copper block.

3 Theoretical Approach to the Dynamic Susceptibility

The surface impedance Z_s, as measured in our experiments, depends on the complex permeability as well as the complex resistivity of the sample. Since here we are investigating a system in the vicinity of, and at, its ferromagnetic phase transition, the permeability will play an important role in our measurements of Z_s. Theoretical approaches to the dynamic susceptibility are well-established [7, 8], but the literature covering this topic as well as the use of the results is unfortunately not consistent with regard to sign conventions, use of SI or cgs system or the extent to which small corrections are kept. Therefore in this chapter I present in detail a derivation of the important results in a way that I will consistently follow throughout this thesis. All formulae are in SI. If values for magnetic fields are given, then they are in units of T/μ_0.

3.1 Equations of Motion

There are different types of equations of motion that describe the interaction of a magnetization with a magnetic field. The starting point is the precession of a magnetization vector $\vec{M}$ in the presence of a magnetic field $\vec{H}$ around this magnetic field, which is described by the following equation:

$$\frac{d\vec{M}}{dt} = \gamma\vec{M} \times \vec{H} \tag{1}$$

Here γ, the gyromagnetic ratio, is a constant: 176 GHz/T.

Now damping of this precessional motion is assumed. Different forms of a damping term were proposed on phenomenological grounds, assuring that the damping will produce a torque which aligns the magnetization with the magnetic

field. The following form gives the so-called Landau-Lifshitz equation [7]:

$$\frac{d\vec{M}}{dt} = \gamma(\vec{M} \times \vec{H}) - \lambda \left(\frac{(\vec{H} \cdot \vec{M})\vec{M}}{|\vec{M}|^2} - \vec{H} \right) \tag{2}$$

Here λ is the Landau-Lifshitz damping parameter which has dimensions of frequency. Using the vector identity

$$\vec{M} \times (\vec{M} \times \vec{H}) = \vec{M}(\vec{H} \cdot \vec{M}) - \vec{H}(\vec{M} \cdot \vec{M}) = \vec{M}(\vec{H} \cdot \vec{M}) - \vec{H}|\vec{M}|^2$$

this equation becomes

$$\frac{d\vec{M}}{dt} = \gamma(\vec{M} \times \vec{H}) - \frac{\lambda}{|\vec{M}|^2}(\vec{M} \times (\vec{M} \times \vec{H})) \tag{3}$$

Now introduce a dimensionless damping parameter α as $\alpha = \frac{\lambda}{\gamma|M|}$. Thus the equation of motion can be written as

$$\frac{d\vec{M}}{dt} = \gamma(\vec{M} \times \vec{H}) - \frac{\alpha\gamma}{|M|}(\vec{M} \times (\vec{M} \times \vec{H})).$$

Now take the vector product of $\vec{M}$ and this equation:

$$\vec{M} \times \frac{d\vec{M}}{dt} = \gamma\vec{M} \times (\vec{M} \times \vec{H}) - \frac{\alpha\gamma}{|M|}\vec{M} \times (\vec{M} \times (\vec{M} \times \vec{H})) \tag{4}$$

Using $\vec{M} \times (\vec{M} \times (\vec{M} \times \vec{H})) = -\vec{M} \times \vec{H}(\vec{M} \cdot \vec{M}) = -|\vec{M}|^2\vec{M} \times \vec{H}$ this equation can be expressed as

$$\vec{M} \times \frac{d\vec{M}}{dt} = \gamma\vec{M} \times (\vec{M} \times \vec{H}) + \alpha\gamma|M|\vec{M} \times \vec{H}.$$

This is equivalent to

$$\gamma\vec{M} \times (\vec{M} \times \vec{H}) = \vec{M} \times \frac{d\vec{M}}{dt} - \alpha\gamma|M|\vec{M} \times \vec{H}.$$

If you plug this into the above equation (3.1) of motion you get

$$\frac{d\vec{M}}{dt} = \gamma(\vec{M} \times \vec{H}) - \frac{\alpha}{|M|}\left(\vec{M} \times \frac{d\vec{M}}{dt} - \alpha\gamma|M|(\vec{M} \times \vec{H}) \right)$$

which is equivalent to

$$\frac{d\vec{M}}{dt} = \gamma(1 + \alpha^2)(\vec{M} \times \vec{H}) - \frac{\alpha}{|M|}\left(\vec{M} \times \frac{d\vec{M}}{dt} \right) \tag{5}$$

This is the Gilbert equation of motion with the dimensionless Gilbert damping parameter α.

As is seen clearly in this equation, the change of $\vec{M}$ with time is always perpendicular to $\vec{M}$. Thus the absolute value of $\vec{M}$ does not change, only its orientation. This change is the precession described by the first term and the damping due to the second term, which will cause the magnetization to align with the magnetic field, spiraling around the magnetic field. This is schematically shown in figure (3).

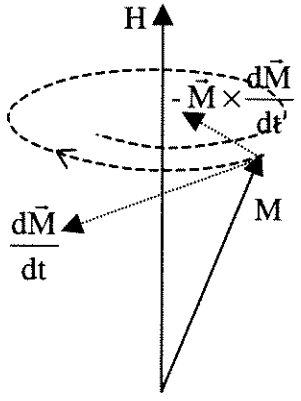

Figure 3: Damped precession of the magnetization around the magnetic field

3.2 Dynamic Susceptibility

To extract the dynamic susceptibility χ, which is defined by $\vec{m} = \chi\vec{h}$ with dynamic magnetization $\vec{m}$ and dynamic magnetic field $\vec{h}$, assume the following forms of the overall magnetic field and magnetization:

$$\vec{H}(t) = \hat{z}H_i + \vec{h}_i e^{i\omega t} \text{ where } \hat{z} \perp \vec{h}_i$$
$$\vec{M}(t) = \hat{z}M_0 + \vec{m}e^{i\omega t} \text{ where } \hat{z} \perp \vec{m}$$

Here M_0 is the static magnetization and H_i is the internal magnetic field, which has to be distinguished from the applied field H_0. Furthermore it will be assumed

that the static magnetic field and the static magnetization are much larger than their dynamic counterparts:

$$|\vec{H}| \gg |\vec{h}_i| \text{ and } |\vec{M}| \gg |\vec{m}|.$$

Only first order terms in $\vec{h}_i$ and $\vec{m}$ will be kept. With this configuration the different terms in the equation of motion become:

$$\frac{d\vec{M}}{dt} = i\omega e^{i\omega t}\vec{m} = i\omega e^{i\omega t}\begin{pmatrix} m_x \\ m_y \\ 0 \end{pmatrix}$$

$$\begin{aligned} \vec{M} \times \vec{H} &= (\hat{z}M_0 + \vec{m}e^{i\omega t}) \times (\hat{z}H_i + \vec{h}_i e^{i\omega t}) = M_0 e^{i\omega t}(\hat{z} \times \vec{h}_i) + H_i e^{i\omega t}(\vec{m} \times \hat{z}) \\ &= M_0 e^{i\omega t}\begin{pmatrix} -h_{iy} \\ h_{ix} \\ 0 \end{pmatrix} + H_i e^{i\omega t}\begin{pmatrix} m_y \\ -m_x \\ 0 \end{pmatrix} \end{aligned}$$

$$\vec{M} \times \frac{d\vec{M}}{dt} = (\hat{z}M_0 + \vec{m}e^{i\omega t}) \times i\omega e^{i\omega t}\vec{m} = M_0 i\omega e^{i\omega t}(\hat{z} \times \vec{m}) = M_0 i\omega e^{i\omega t}\begin{pmatrix} -m_y \\ m_x \\ 0 \end{pmatrix}$$

Thus the Gilbert equation (5) becomes

$$\begin{aligned} i\omega e^{i\omega t}\begin{pmatrix} m_x \\ m_y \\ 0 \end{pmatrix} &= \gamma(1+\alpha^2)\left(M_0 e^{i\omega t}\begin{pmatrix} -h_{iy} \\ h_{ix} \\ 0 \end{pmatrix} + H_i e^{i\omega t}\begin{pmatrix} m_y \\ -m_x \\ 0 \end{pmatrix}\right) \\ &\quad -\frac{\alpha}{M}\left(M_0 i\omega e^{i\omega t}\begin{pmatrix} -m_y \\ m_x \\ 0 \end{pmatrix}\right) \end{aligned} \tag{6}$$

Since $|\vec{m}| \ll |\vec{M}_0|$, one has $\frac{M_0}{M} \approx 1$ and this becomes

$$i\omega \begin{pmatrix} m_x \\ m_y \\ 0 \end{pmatrix} = \gamma(1+\alpha^2) \left(M_0 \begin{pmatrix} -h_{iy} \\ h_{ix} \\ 0 \end{pmatrix} + H_i \begin{pmatrix} m_y \\ -m_x \\ 0 \end{pmatrix} \right) - \alpha i\omega \begin{pmatrix} -m_y \\ m_x \\ 0 \end{pmatrix} \quad (7)$$

Now we must clearly distinguish the internal magnetic field with respect to the external field and the demagnetization field. If a magnetized sample is placed inside a magnetic field, the magnetization will orient parallel to the applied field. But this means that the magnetic field caused by the magnetization inside the sample, the demagnetization field, will be antiparallel to the external field. Thus the effective magnetic field inside the sample will be the superposition of the external and the demagnetization field. The size of the demagnetization field is determined by the magnetization and the sample geometry. Therefore the k-component h_{ik} of the dynamic internal magnetic field is given by

$$h_{ik} = h_k - N_k m_k$$

where N_k is the demagnetization factor with respect to the k-axis and is only geometry dependent, h_k is the k-component of the applied dynamic magnetic field, In the same way $H_i = H_0 - N_z M_0$, where H_0 is the applied static magnetic field. Thus equation (7) becomes

$$\begin{aligned} i\omega \begin{pmatrix} m_x \\ m_y \\ 0 \end{pmatrix} &= \gamma(1+\alpha^2) \left(M_0 \begin{pmatrix} -h_y + N_y m_y \\ h_x - N_x m_x \\ 0 \end{pmatrix} + (H_0 - N_z M_0) \begin{pmatrix} m_y \\ -m_x \\ 0 \end{pmatrix} \right) \\ &\quad - \alpha i\omega \begin{pmatrix} -m_y \\ m_x \\ 0 \end{pmatrix} \end{aligned}$$

$$
i\omega \begin{pmatrix} m_x \\ m_y \\ 0 \end{pmatrix} = \gamma(1+\alpha^2)M_0 \begin{pmatrix} -h_y + N_y m_y \\ h_x - N_x m_x \\ 0 \end{pmatrix}
$$

$$
+(\gamma(1+\alpha^2)(H_0 - N_z M_0) + i\alpha\omega) \begin{pmatrix} m_y \\ -m_x \\ 0 \end{pmatrix} \tag{8}
$$

Now define two frequencies corresponding to the static magnetization and the static internal magnetic field:

$$\omega_M = \gamma(1+\alpha^2)M_0 \tag{9}$$

$$\omega_0 = \gamma(1+\alpha^2)(H_0 - N_z M_0) \tag{10}$$

Then Eq. (8) reads

$$
i\omega \begin{pmatrix} m_x \\ m_y \\ 0 \end{pmatrix} = \omega_M \begin{pmatrix} -h_y + N_y m_y \\ h_x - N_x m_x \\ 0 \end{pmatrix} + (\omega_0 + i\alpha\omega) \begin{pmatrix} m_y \\ -m_x \\ 0 \end{pmatrix} \tag{11}
$$

Thus equations for the x- and y-components are found. Using

$$\Gamma = \alpha\omega$$

they are:

$$i\omega m_x = -\omega_M h_y + (\omega_M N_y + \omega_0 + i\Gamma)m_y$$

$$i\omega m_y = \omega_M h_x - (\omega_M N_x + \omega_0 + i\Gamma)m_x$$

Now combine these two equations:

$$
\begin{aligned}
(i\omega)^2 m_x &= -i\omega\omega_M h_y + (\omega_M N_y + \omega_0 + i\Gamma)i\omega m_y \\
&= -i\omega\omega_M h_y + (\omega_M N_y + \omega_0 + i\Gamma)(\omega_M h_x - (\omega_M N_x + \omega_0 + i\Gamma)m_x) \\
&= -i\omega\omega_M h_y + \omega_M(\omega_M N_y + \omega_0 + i\Gamma)h_x \\
&\quad -(\omega_M N_y + \omega_0 + i\Gamma)(\omega_M N_x + \omega_0 + i\Gamma)m_x
\end{aligned}
$$

Now set

$$\begin{aligned}\omega_r^2 &= (\omega_M N_y + \omega_0)(\omega_M N_x + \omega_0) \\ &= \gamma^2(1+\alpha^2)^2(H_0 + M_0(N_y - N_z))(H_0 + M_0(N_x - N_z)) \end{aligned} \tag{12}$$

Then one obtains

$$\begin{aligned}-\omega^2 m_x &= -\omega_M h_y i\omega + \omega_M(\omega_M N_y + \omega_0 + i\Gamma)h_x \\ &\quad -(\omega_r^2 + i\Gamma(\omega_M(N_x + N_y) + 2\omega_0) - \alpha^2\omega^2)m_x \end{aligned}$$

$$\begin{aligned}\Leftrightarrow \quad &(\omega_r^2 - (1+\alpha^2) + i\Gamma(\omega_M(N_x + N_y) + 2\omega_0))m_x \\ &= \omega_M(\omega_M N_y + \omega_0 + i\Gamma)h_x - i\omega_M\omega h_y \end{aligned}$$

Now the susceptibility can be obtained. The susceptibility tensor is defined as

$$\vec{m} = \overline{\overline{\chi}}\vec{h} \tag{13}$$

Thus the components of the susceptibility tensor that relate the x- and y-components of $\vec{h_i}$ and $\vec{m}$ have been obtained:

$$\chi_{xx} = \frac{\omega_M(\omega_M N_y + \omega_0 + i\Gamma)}{\omega_r^2 - (1+\alpha^2)\omega^2 + i\Gamma(2\omega_0 + \omega_M(N_x + N_y))} \tag{14}$$

$$\chi_{xy} = \frac{-i\omega_M\omega}{\omega_r^2 - (1+\alpha^2)\omega^2 + i\Gamma(2\omega_0 + \omega_M(N_x + N_y))} \tag{15}$$

$$\chi_{yy} = \frac{\omega_M(\omega_M N_x + \omega_0 + i\Gamma)}{\omega_r^2 - (1+\alpha^2)\omega^2 + i\Gamma(2\omega_0 + \omega_M(N_x + N_y))} \tag{16}$$

$$\chi_{yx} = -\chi_{xy} = \frac{i\omega_M\omega}{\omega_r^2 - (1+\alpha^2)\omega^2 + i\Gamma(2\omega_0 + \omega_M(N_x + N_y))} \tag{17}$$

From the susceptibility χ the permeability μ can be obtained using the relation $\mu/\mu_0 = \chi + 1$. The complex quantity μ can be split into real and imaginary parts $\mu = \mu_1 - i\mu_2$. From now on consider only χ_{xx}. Then μ is given by:

$$\begin{aligned}\mu_1/\mu_0 = &\frac{(\omega_r^2 - (1+\alpha^2)\omega^2)(\omega_M(\omega_M N_y + \omega_0) + \omega_r^2 - (1+\alpha^2)\omega^2)}{(\omega_r^2 - (1+\alpha^2)\omega^2)^2 + (\Gamma(2\omega_0 + \omega_M(N_x + N_y)))^2} \\ &+\frac{\Gamma^2(\omega_M + 2\omega_0 + \omega_M(N_x + N_y))(2\omega_0 + \omega_M(N_x + N_y))}{(\omega_r^2 - (1+\alpha^2)\omega^2)^2 + (\Gamma(2\omega_0 + \omega_M(N_x + N_y)))^2} \end{aligned} \tag{18}$$

$$\mu_2/\mu_0 = \frac{\Gamma(\omega_M(\omega_r^2 - (1+\alpha^2)\omega^2) - \omega_M(\omega_M N_y + \omega_0)(2\omega_0 + \omega_M(N_x + N_y)))}{(\omega_r^2 - (1+\alpha^2)\omega^2)^2 + (\Gamma(2\omega_0 + \omega_M(N_x + N_y)))^2} \quad (19)$$

The frequency dependences of μ_1 and μ_2 for parameters that resemble those of our experiments are shown in figure (4) for typical values of magnetic field and magnetization. The characteristic features of these curves will be the topic of the next two sections.

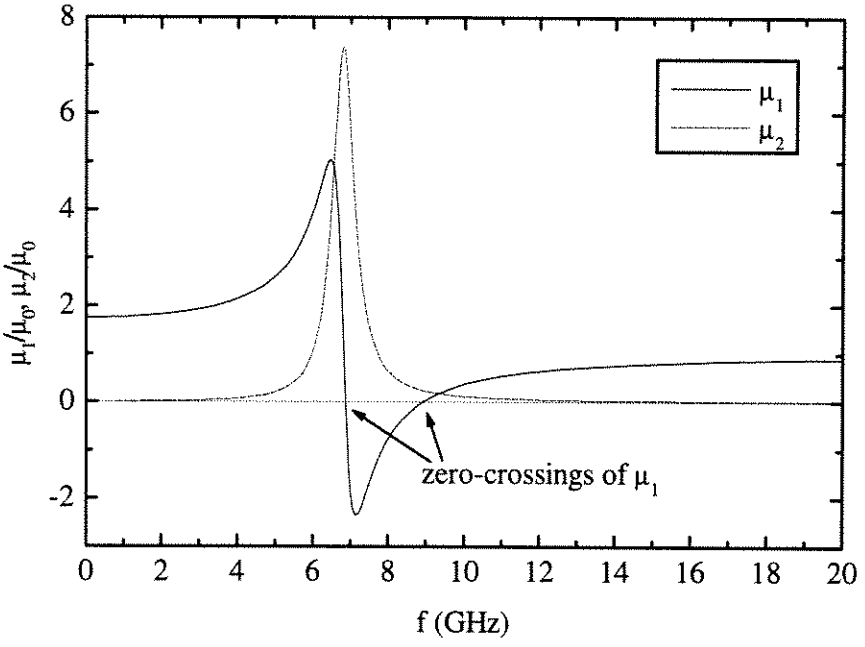

Figure 4: Frequency dependence of calculated permeability for an applied field parallel to the sample ($\mu_0 H_0 = 0.2T$, $\mu_0 M_0 = 0.15T$, $N_z = N_x = 0.125$, $N_y = 0.75$, $\alpha = 0.05$, $\Gamma_0 = 0$)

3.3 Ferromagnetic Resonance (FMR)

There are two distinct features that will be the focus of the further investigation and are therefore discussed here in more detail. First there is a resonant

peak in $\mu_2(\omega, \mathrm{H})$, combined with a zero-crossing from a large positive to a large negative value in $\mu_1(\omega, \mathrm{H})$. These features in μ cause the ferromagnetic resonance (FMR), an effect easily observable experimentally as a peak in the surface resistance $\mathrm{R_s}$. The resonant frequency can be found by examining the expression (19) for μ_2, searching for a frequency where the value of μ_2 becomes large. First assume that α is small. Therefore the terms containing Γ will only be of importance if the other ones also become very small. (Therefore the numerator of Eq. (19) for μ_2 is generally small. The denominator on the other hand contains a term without Γ, Therefore the values for μ_2 will be very small unless this term in the denominator vanishes, which is the case for the resonance.) Thus the resonance requires that the first term in the denominator of μ_2 vanishes:

$$\omega_\mathrm{r}^2 - (1 + \alpha^2)\omega^2 = 0 \tag{20}$$

From now on neglect the α^2 term since other term of this order in Eqs.(18) and (19) are also neglected to find the FMR and FMAR frequencies. Thus the FMR condition becomes:

$$\omega = \omega_\mathrm{r} \tag{21}$$

If the condition (21) holds, the denominator will only be the small, constant, second term and since the numerator also has a constant, but bigger term, the overall μ_2 will become large. Therefore equation (21) gives the resonance condition, or in terms of the magnetic fields:

$$\omega_\mathrm{r} = \gamma\sqrt{((\mathrm{N_y} - \mathrm{N_z})\mathrm{M_0} + \mathrm{H_0})((\mathrm{N_x} - \mathrm{N_z})\mathrm{M_0} + \mathrm{H_0})} \tag{22}$$

The demagnetization factors have been calculated for special geometries like ellipsoids [7]. Our sample is a thin disk that may be approximated by an ellipsoid of the same dimensions. But even the idealization of an infinitely thin, infinitely wide flat sample, for which Eq.(22) simplifies much more, will give a first

prediction of the qualitative behavior. In this case, if the external magnetic field is applied parallel to the disk ($\hat{y} \perp$ disk) one has $N_y = 1,\ N_x = N_z = 0$ and therefore

$$\omega_r = \gamma\sqrt{(M_0 + H_0)H_0} \qquad \vec{H}_0 \parallel \text{infinite disk} \tag{23}$$

If the field is applied perpendicular to the thin disk ($\hat{z} \perp$ disk), the demagnetization factors are $N_z = 1, N_x = N_y = 0$ and therefore the FMR condition is:

$$\omega_r = \gamma\,|H_0 - M_0| \qquad \vec{H}_0 \perp \text{infinite disk} \tag{24}$$

Thus the FMR frequency is sensitive to both the sample magnetization and the applied magnetic field.

3.4 Ferromagnetic Antiresonance (FMAR)

The second interesting feature occurs at the second zero crossing of μ_1 (compare figure (4)). The first zero crossing is at the resonance, the second causes a minimum of the surface resistance, called ferromagnetic antiresonance (FMAR). (In the case $\mu_1 \ll \mu_2$ the surface resistance is approximately $R_s \approx \sqrt{\omega\rho\mu_2}(1 + \frac{1}{8}(\frac{\mu_1}{\mu_2})^2)$, thus a zero in μ_1 will result in a minimum in R_s.) This second zero crossing can be found from the expression (18) for μ_1. Again first neglect all terms which have α^2 in them. Then set the numerator equal to zero:

$$(\omega_r^2 - \omega^2)\left(\omega_M(\omega_M N_y + \omega_0) + (\omega_r^2 - \omega^2)\right) = 0 \tag{25}$$

The first factor vanishes at the resonance frequency found above, the second factor vanishes at the antiresonance. Therefore the FMAR condition is

$$\omega_{ar}^2 = \omega_M(\omega_M N_y + \omega_0) + \omega_r^2 \tag{26}$$

Expressed as a condition in terms of magnetic fields:

$$\omega_{ar} = \gamma\sqrt{(M_0(N_y - N_z) + H_0)(M_0(N_x - N_z + 1) + H_0)}. \tag{27}$$

This term can be simplified for the two special cases discussed above. In the case with the field parallel to the plate:

$$\omega_{ar} = \gamma(M_0 + H_0) \qquad \vec{H}_0 \parallel \text{infinite disk} \tag{28}$$

For the thin plate with the field perpendicular to the plate:

$$\omega_{ar} = \gamma\sqrt{H_0(H_0 - M_0)} \qquad \vec{H}_0 \perp \text{infinite disk} \tag{29}$$

3.5 Surface Impedance

The quantity that we extract from the experiment is the complex surface impedance $Z_s = R_s - iX_s$, which is coupled to the permeability μ as: $Z_s = \sqrt{i\omega\mu\rho}$. Here ρ is the resistivity, in general a complex, frequency dependent quantity. But since the sample is a rather poor conductor, ρ can approximately be considered real and frequency independent at microwave frequencies. Therefore assuming ρ to equal the dc resistivity, it is possible to calculate the frequency dependence of R_s and X_s on the basis of the relationship above and the frequency dependence of μ. This is shown in figure (5) for the same parameters as above. Here the FMR clearly shows up as a peak in R_s and a sharp drop in X_s , and the FMAR is visible as a minimum in R_s and a step in X_s, both on top of an overall frequency behavior of Z_s dominated by a $\sqrt{\omega}$ dependence.

Thus we have seen, that the characteristic features of μ will cause strong features in Z_s. These characteristics in Z_s are therefore evidence that the conditions for FMR and FMAR are fulfilled. These FMR and FMAR conditions involve the frequency, the magnetic field, and the magnetization as variables. In our experiment the frequency can be chosen freely in a broad frequency range. An external magnetic field can be applied and for the case that the field is parallel to the sample disk the field can also be changed continuously in some range. The magnetization of the sample is a function of the applied field and the temperature,

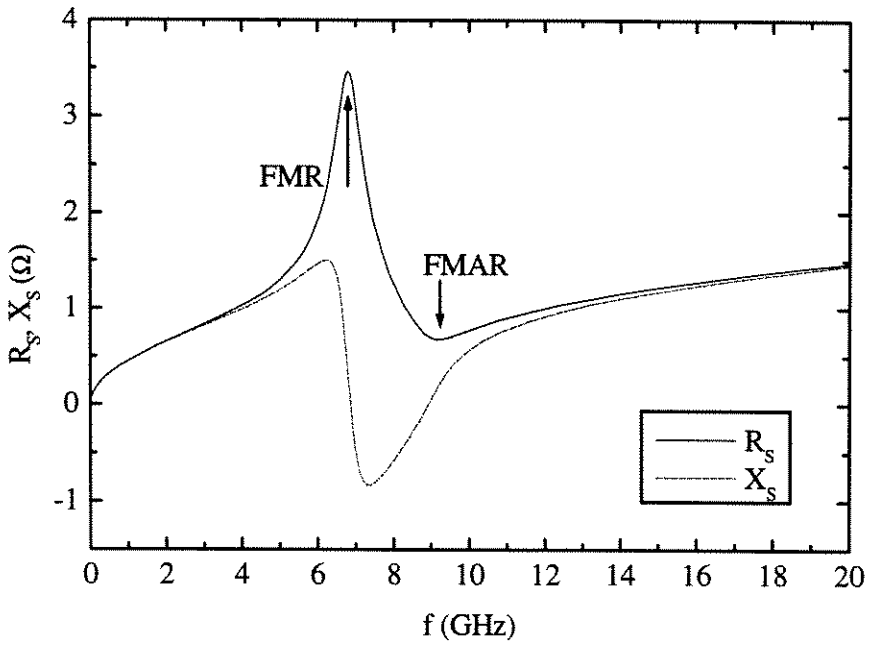

Figure 5: Frequency dependence of calculated surface impedance for an applied field parallel to the sample ($\mu_0 H_0 = 0.2\,\mathrm{T}$, $\mu_0 M_0 = 0.15\,\mathrm{T}$, $N_z = N_x = 0.125$, $N_y = 0.75$, $\alpha = 0.05$, $\rho_{dc} = 3 \cdot 10^{-5}\Omega\mathrm{m}$, $\Gamma_0 = 0$). The FMR is slightly below 7 GHz, the FMAR around 9 GHz.

parameters that can be controlled during the experiment. A main part of the experimental results will therefore be the behavior of FMR and FMAR depending on frequency, temperature and external magnetic field.

3.6 Resonance Linewidth

The FMR causes a peak in R_s, the position of which is given by the FMR condition. The width of this peak, the ferromagnetic resonance linewidth Γ is given by $\Gamma = \alpha\omega$. This frequency dependence would cause a linewidth of zero in the limit of zero frequency. But in real systems, the resonance linewidth will never vanish exactly since in a finite sample the internal magnetic field will not be completely uniform. To take this into account [9], a phenomenological zero

frequency linewidth Γ_0 can be introduced as a constant into the model by now defining the resonance linewidth as $\Gamma = \alpha\omega + \Gamma_0$.

3.7 The Case of Zero External Field

A substantial part of the measurements presented here were performed without applying an external field. In this case the theory described above cannot *a priori* be expected to work, since the starting point was the precession of the magnetization around the magnetic field. But the theory only assumes that a magnetic field is present, without any restriction to the origin of the field. However, in the presence of a magnetization there will always be internal magnetic fields, e.g. originating from an inhomogeneous domain structure, and therefore the model might also apply for this case.

In fact the predictions of the model for the case of the thin plate with the magnetic field parallel to the plate, in the limit of the field strength going to zero, seem to agree well with the experimental results. The frequency dependence of Z_s, calculated with parameters close to those of our experiment in zero field, is shown in figure (6). Here the antiresonance is still clearly visible as a minimum in R_s and an increase in X_s. Assuming a temperature dependence of the magnetization and the resistivity [10], it is also possible to calculate the temperature dependence of Z_s for a fixed frequency. This is shown in figure (7) for a frequency of 8 GHz. The antiresonance is visible as a minimum in R_s also in the temperature dependence and as an increase in X_s. The condition for the antiresonance in this case, $\omega = \gamma M_0$ thus gives the same features in the temperature dependence that were already seen in the frequency dependence of Z_s.

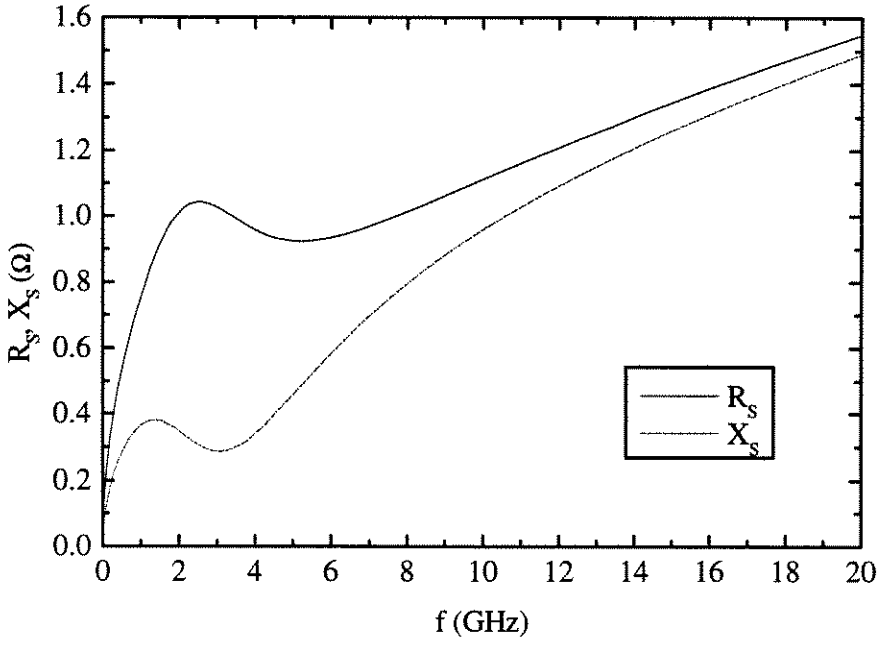

Figure 6: Calculated frequency dependence of surface impedance for zero external field ($\mu_0 H_0 = 0$, $\mu_0 M_0 = 0.5\,\mathrm{T}$, $N_z = N_x = 0.125$, $N_y = 0.75$, $\alpha = 0.05$, $\rho_{dc} = 3 \cdot 10^{-5}\,\Omega\mathrm{m}$, $\Gamma_0 = 2\pi \cdot 2.5\,\mathrm{GHz}$)

3.8 FMR and FMAR for the Non Ideal Case

Since the calculations described above do not accurately reflect our actual measurements in several respects, modifications will be introduced to help describe the characteristics that are found in the experiments. The model assumes that the magnetization and the magnetic field are uniform throughout the sample in such a way that the static magnetic field and the static magnetization are parallel, as are their dynamic counterparts. In reality this will be true only if the applied external field is strong enough to magnetize the sample uniformly. For our experiments this will only be the case for measurements with a considerable applied field very close to or above T_C. The majority of the data presented here does not fit in this category.

In our experiment we have two main differences compared to the geometry

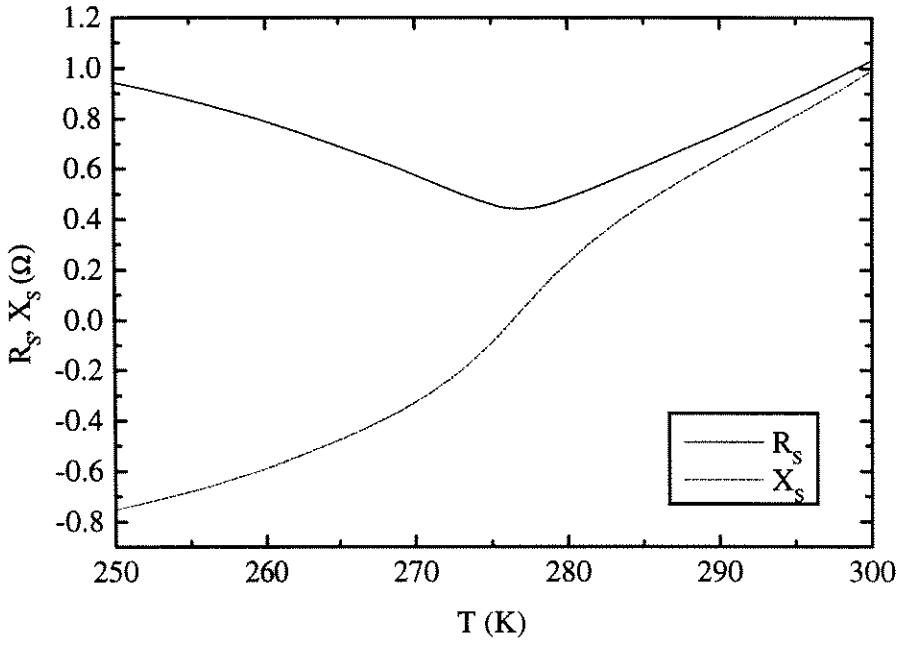

Figure 7: Calculated temperature dependence of surface impedance for zero external field ($\mu_0 H_0 = 0$, $\mu_0 M = 0.5\,T$, $N_z = N_x = 0.125$, $N_y = 0.75$, $\alpha = 0.05$, $\Gamma_0 = 0, f = 8\,GHz$)

of the model. First our magnetization may not be uniform. For small external fields our sample will be divided into magnetic domains with different orientations. Second our dynamic applied magnetic field is not uniform, since we use the Corbino geometry and therefore at different parts of the Corbino disk the high frequency field will have different directions, whereas the magnitude will be the same. The latter difference will exclude that even for the highest applied static fields the model can strictly be expected to hold.

Nevertheless the model might work locally. For small regions of the sample the high frequency field is uniform as might be the magnetization and the static magnetic field. Therefore it is essential to consider the model for such a case.

One necessary modification is the use of the demagnetization factors. The demagnetization in z-direction, parallel to the static field, was only used to express the internal magnetic field H_i as $H_i = H_0 - N_z M_0$. Here M_0 is the net magnetization

of the sample. But as mentioned, we want to consider a local response instead of an overall one. Therefore one should keep the internal field H_i and consider the changes of this internal field separately. The demagnetization factors in x- and y-direction were introduced because the dynamic magnetic fields might be affected by dynamic demagnetization fields. This might be the case, but since we consider local effects now, the global shape of the sample will not affect this dynamic demagnetization. Thus it makes sense to replace the terms $N_y M_0$ and $N_x M_0$ by $N'_y M_0$ and $N'_x M_0$, where the primed demagnetization factors and the magnetization are the appropriate local quantities. With these changes the FMR and FMAR conditions become:

$$\omega_r = \gamma\sqrt{(N'_y M_0 + H_i)(N'_x M_0 + H_i)} \tag{30}$$

$$\omega_{ar} = \gamma\sqrt{(N'_y M_0 + H_i)((N'_x + 1)M_0 + H_i)} \tag{31}$$

These formulae are more general than those given earlier since for the uniform case the local quantities equal the global ones and thus the local equations become the global ones.

The global demagnetization factors are determined by the sample geometry. To estimate the global demagnetization factors of our sample, it might be approximated by an oblate ellipsoid with the same ratios of height, width, and length. The demagnetization factors for ellipsoids have been calculated [7] and give for our case the demagnetization factors 3/4, 1/8, 1/8 whereas for the infinitely thin sample they would be 1, 0, 0.

4 The Material under Study: $La_{0.8}Sr_{0.2}MnO_3$

4.1 The LSMO-Compounds

The different compounds of the type $La_{1-x}Sr_xMnO_3$ form premiere examples of the materials that exhibit colossal magnetoresistance (CMR). The magnetic and electronic phases differ depending on the level of doping [11]. For a doping level x higher than approximately 0.17, the material is a ferromagnetic metal at low temperatures, whereas for $0.08 < x < 0.17$ it is a ferromagnetic insulator. The Curie temperature T_C changes from below 150 K for x=0.1 to higher than 350 K for x between 0.3 and 0.4. At temperatures around T_C the resistivity increases steeply. But compounds with $x < 0.26$ show the opposite behavior above T_C. There the resistivity decreases with increasing temperature, a semiconductor-like or insulator-like characteristic.

The compound of our experiments, $La_{0.8}Sr_{0.2}MnO_3$, has a T_C of around 300 K, which is close to the highest temperature accessible with our current experimental setup. The sample of the present study is a single-crystal grown by the floating-zone technique [12]. A very similar sample was studied previously by different groups [13]. The resistivity for low temperatures is metallic, increasing very steeply around 300 K. Around 320 K the resistivity is maximal and for higher temperatures the resistivity decreases in a semiconducting fashion. The magnetization has been studied by different techniques and $T_C$was determined to be around 302 K.

4.2 The Sample

The data described in this thesis were all taken from the same sample. It is disk shaped with a diameter of 3.9 mm and a thickness of 0.82 mm. A photograph showing the Corbino disk of the sample with the two gold contacts, corresponding

to inner and outer conductor of the probe, is reproduced in figure 8. The dc

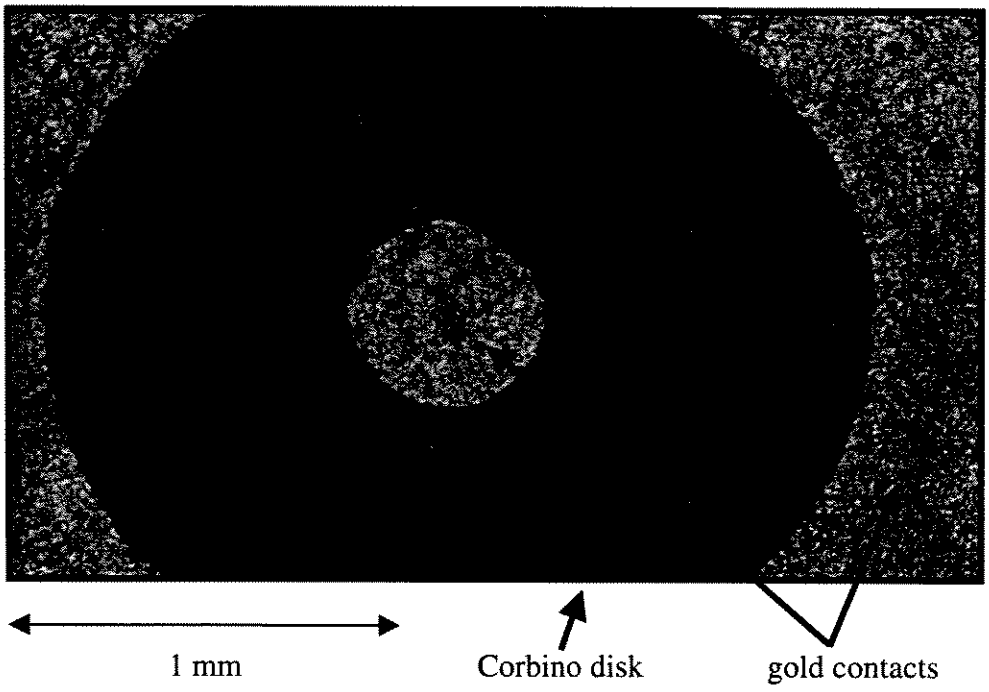

Figure 8: The Corbino disk of the $La_{0.8}Sr_{0.2}MnO_3$ sample with the gold contacts.

resistance measurements that were conducted during the microwave experiments are reproduced in figure (9) for the case of zero and finite external magnetic field, for comparison figure (10) shows the resistivity data from [13].

Since the dc resistance is measured in a two-point geometry, the resistance of the transmission line and the contacts contribute to the absolute values. But these contributions will be almost temperature independent. Therefore the temperature dependence of the dc resistance can be attributed to the sample.

The sharp increase of the resistivity around 300 K is the dominant feature in the temperature dependence and will contribute an overall shape to the temperature dependence of microwave surface impedance. As seen in figure 9 the dc resistance differs between zero and finite applied field, the sample shows magnetoresistance.

Patrick Fournier conducted susceptibility measurements using a SQUID magnetometer on our particular sample. The magnetization was obtained for the

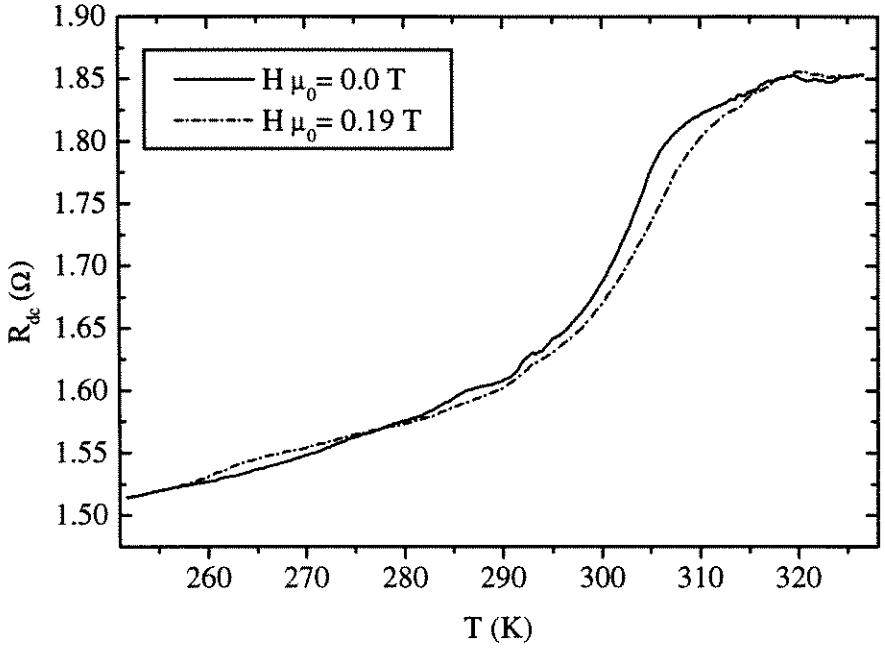

Figure 9: dc resistance of the $La_{0.8}Sr_{0.2}MnO_3$ sample and the coaxial cable probe measured in two point geometry in zero applied field and in 0.19 T magnetic field parallel to the sample disk.

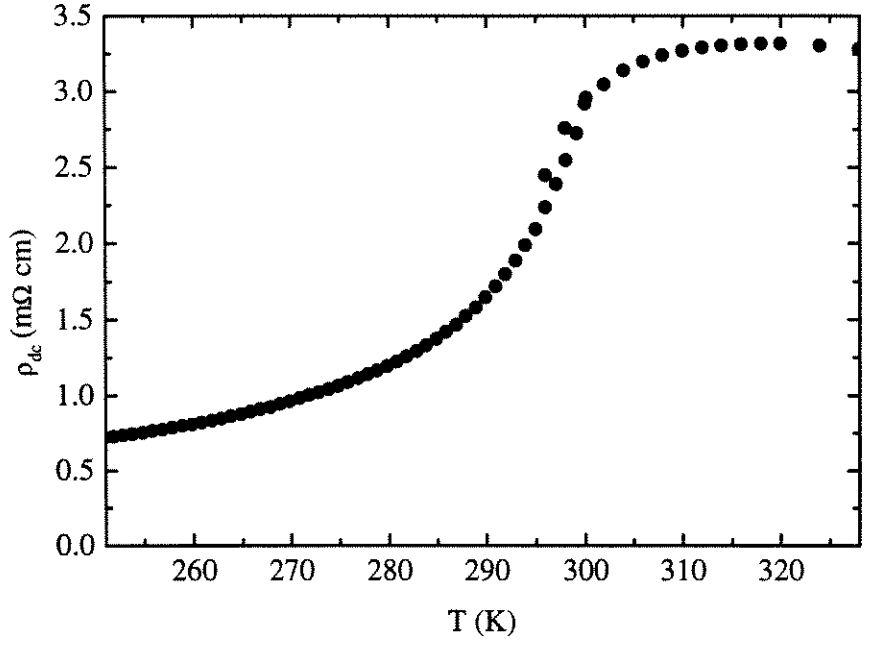

Figure 10: dc resistivity of a similar $La_{0.8}Sr_{0.2}MnO_3$ single crystal sample [13].

case of the applied field perpendicular to the disk as well as for the parallel field. In both cases two different field strengths, 1 mT and 0.2 T, were measured. The results are shown in figure (11).

The magnetization indicates a phase transition from a ferromagnetic to a paramagnetic state with a Curie temperature around 307 K. Thus the magnetic phase transition takes place in the same temperature range as the strong dc resistance changes, a well-known feature of CMR materials. In conclusion the sample seems to be a typical representative of a CMR compound.

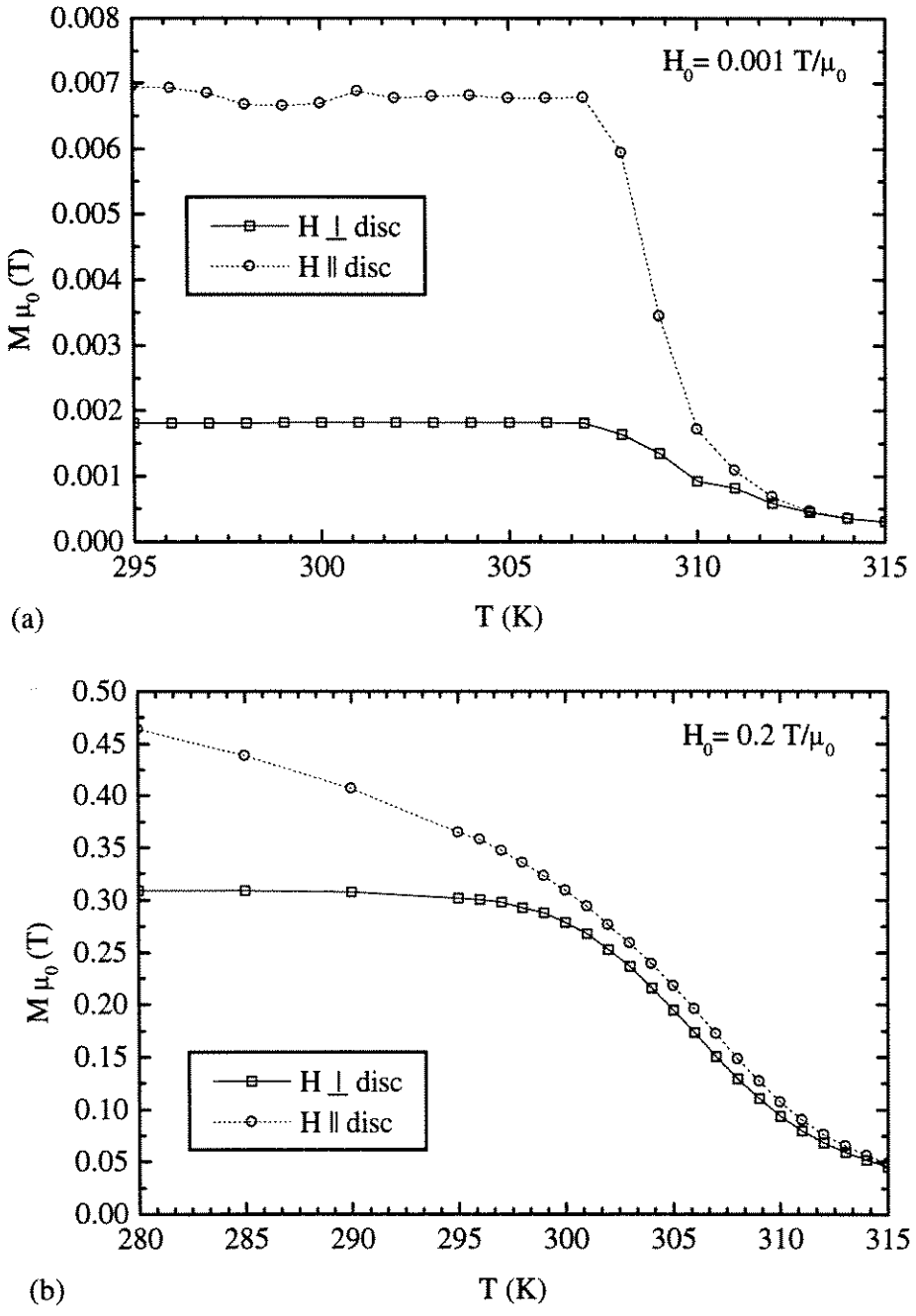

Figure 11: Magnetization of the sample measured with a SQUID magnetometer, (a) in a field of H_0=0.001 T/μ_0, (b) in a field of H_0=0.2 T/μ_0. In both cases the magnetization for the applied field parallel and perpendicular to the sample disk are given.

5 Measurements in Zero Applied Magnetic Field

5.1 Surface Impedance

The first measurements performed were without applying a magnetic field. The frequency dependence of the surface resistance and the surface reactance are plotted in figures (12) and (13).

The overall frequency dependence of R_s and X_s show the characteristic $\sqrt{\omega}$ behavior. In R_s, furthermore, dips can be found for those temperatures which are below 305 K. These are the FMAR minima and therefore they have to vanish as soon as the sample leaves the ferromagnetic state and thus loses its spontaneous magnetization. The existence of FMAR at temperatures of 300 K and the clear absence (visible in the plain $\sqrt{\omega}$ curve at low frequencies) for 310 K gives some first boundaries in the estimation of T_C. For each of these spectra the temperature is different and so is the magnetization below T_C. Therefore the FMAR condition is fulfilled for each of these temperatures at a different frequency, which causes the shift of the minima from one temperature to the next.

In X_s the FMAR is seen as a sharp step at a particular frequency. This frequency is again different for the different temperatures and the frequencies correspond to those found in R_s. The step has disappeared completely at temperatures higher than 305 K. Since X_s has a steep increase for low frequencies anyway, this disappearance of the FMAR feature in X_s is less pronounced than in R_s.

In this plot of X_s versus frequency the curve for 281.8 K does not lie between the two of the next higher and lower temperatures, but below the two. This is due to imperfections in the temperature dependent calibration correction, an issue that will be addressed in chapter 7.

The temperature dependence of the surface resistance and the surface reactance are shown in figure (14) and figure (15), respectively. The temperature

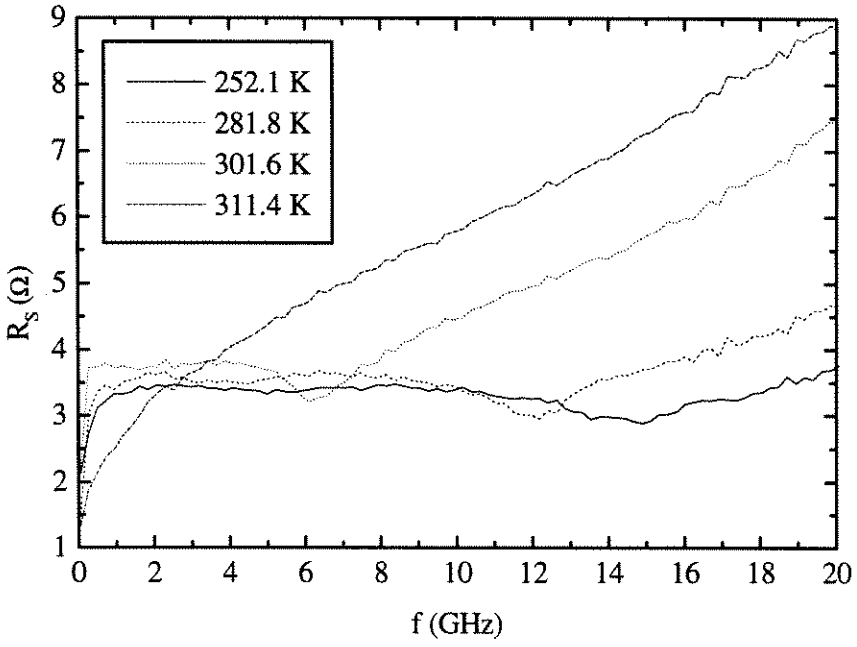

Figure 12: Frequency dependence of the surface resistance of the $La_{0.8}Sr_{0.2}MnO_3$ sample in zero applied magnetic field for four different temperatures

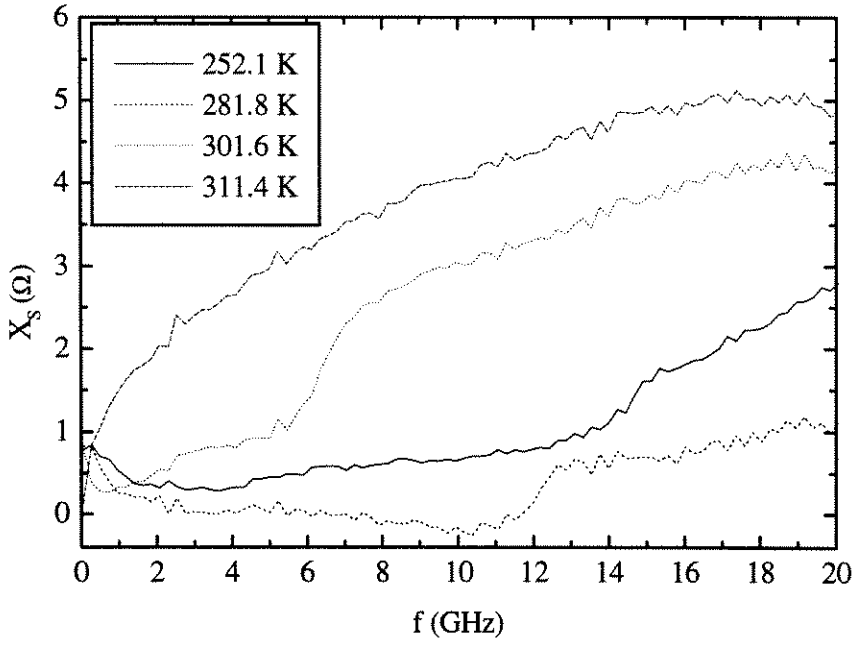

Figure 13: Frequency dependence of the surface reactance of the $La_{0.8}Sr_{0.2}MnO_3$ sample in zero applied magnetic field for four different temperatures

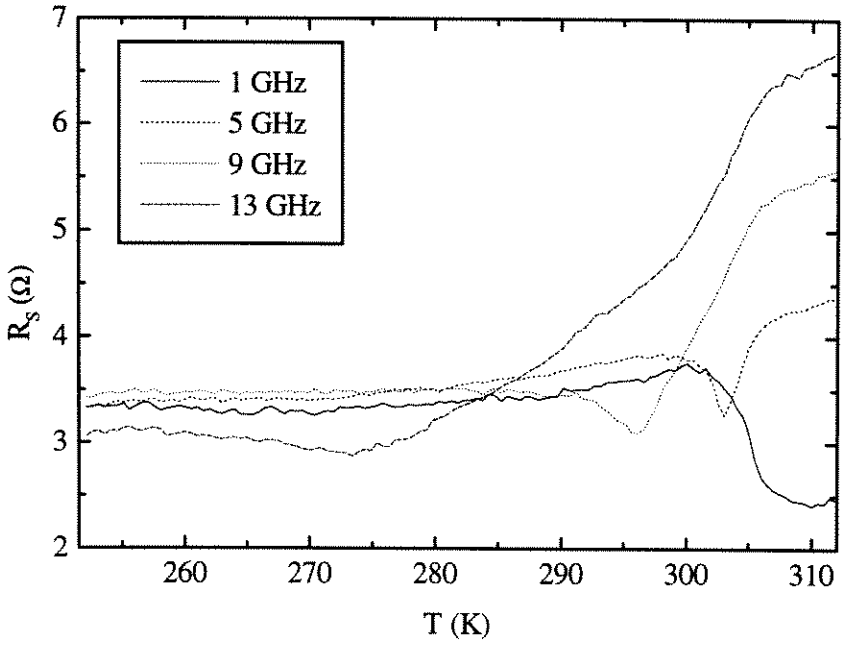

Figure 14: Temperature dependence of the surface resistance of the $La_{0.8}Sr_{0.2}MnO_3$sample in zero applied magnetic field for four different frequencies

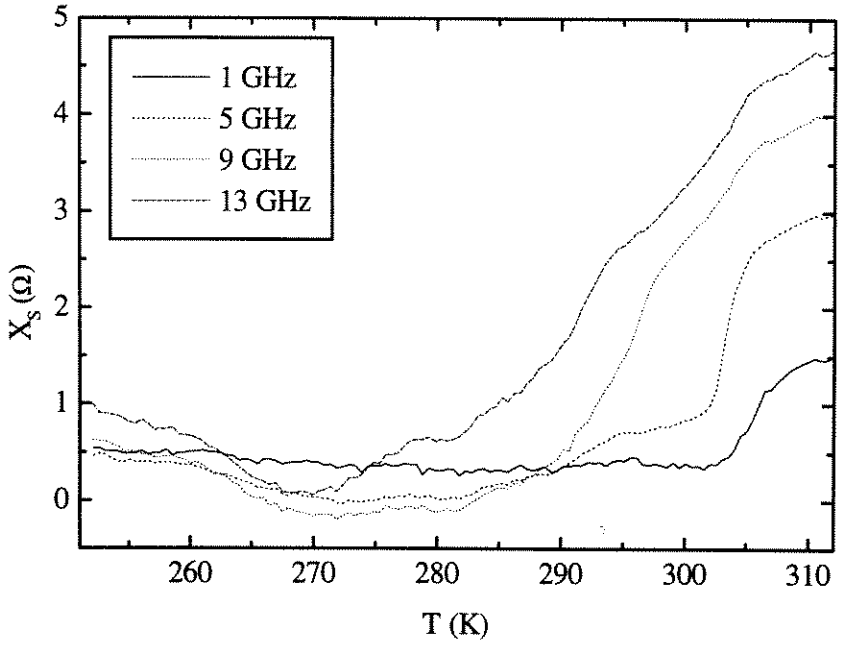

Figure 15: Temperature dependence of the surface reactance of the $La_{0.8}Sr_{0.2}MnO_3$sample in zero applied magnetic field for four different frequencies

dependence of R_s and X_s shows a general increase with increasing temperature. This effect is due to the increase of the resistivity as seen in the dc resistance measurements in figure (9). On top of this general increase R_s shows the minima which are caused by FMAR. Since in the temperature dependence curves the frequencies are different, FMAR occurs at different temperatures. In X_s we again see an overall increase combined with the characteristic steps due to FMAR.

For temperatures well above T_C no magnetization is present and therefore Z_s is not influenced by magnetic behavior anymore. As the $\sqrt{\omega}$ behavior was seen in the frequency spectra, in the temperature dependence the curves for the different frequencies show the same behavior, i.e. their temperature dependence is the same for all frequencies. The temperature where they start to line up like this therefore also has to be close to T_C.

5.2 Spontaneous Magnetization from FMAR

5.2.1 FMAR

As seen in the results of the model for the dynamic susceptibility and in the zero field data, the effect of FMAR shows up as a minimum in the surface resistance R_s and a sharp increase in the surface reactance $X_s(\omega)$. The condition for the FMAR to occur in the case of no applied field is $\omega/\gamma = M_0$. (Again I want to stress that this formula is the limit for H approaching zero for an infinitely thin disk sample with H parallel to the disk. A justification that this procedure is valid will be given in the later chapter about the field dependent measurements with the field parallel to the sample.)

Thus the magnetization of the sample and the frequency of the FMAR are directly related. For a single temperature, corresponding to a specific spontaneous magnetization, the FMAR condition will be fulfilled at a particular frequency, for a single frequency FMAR will occur for a specific temperature. Therefore the

spontaneous magnetization of the sample can be found by determining the position of the antiresonance. To get a first impression of how the position of the FMAR depends on temperature, the complete temperature and frequency dependence of R_s is shown as a gray scale plot in figure (16). Here the FMAR shows up as

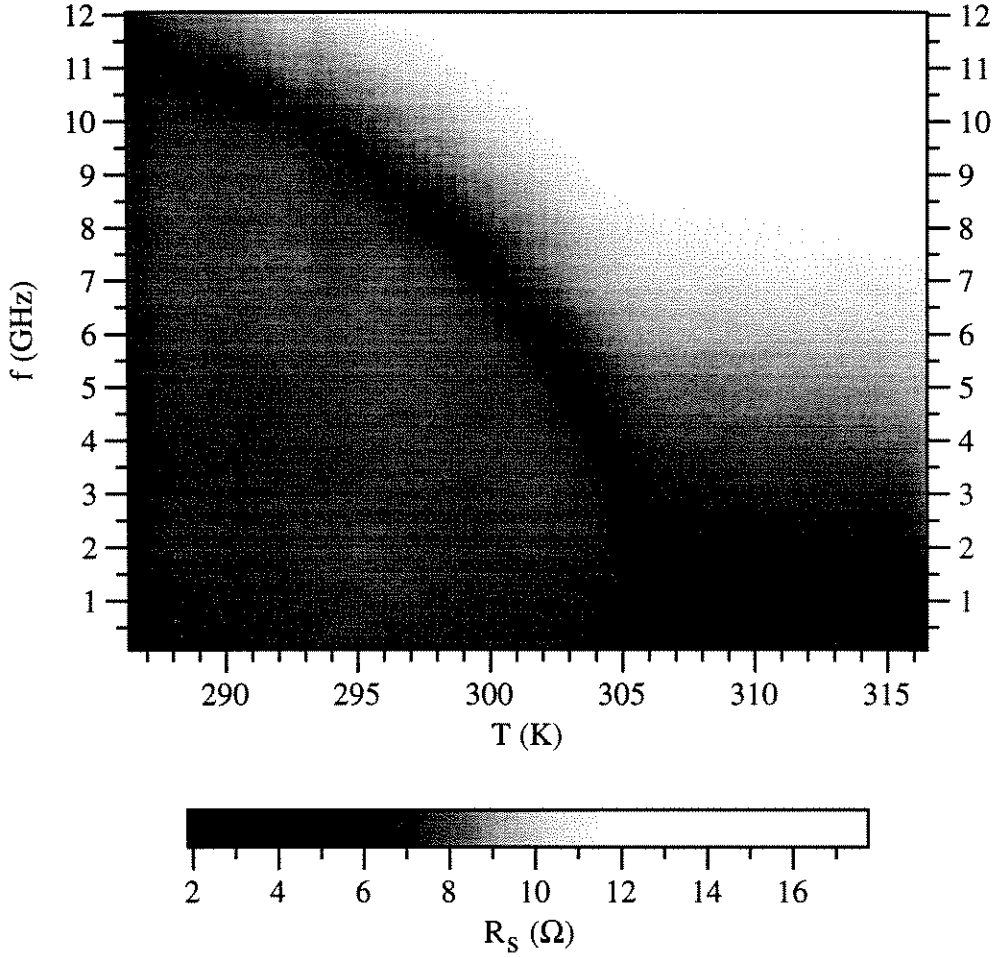

Figure 16: Gray scale plot of R_s as a function of temperature and frequency. The FMAR is the dark curve.

the minimum in R_s that can be seen from a frequency of around 12 GHz at low temperatures until it vanishes at zero frequency around 306 K.

To pinpoint the position of the FMAR the minima in R_s and the steps in X_s were identified in the frequency spectra as well as in the temperature dependent data. Thus there are four different ways to determine the position of the antires-

onance. The frequency of the antiresonance is proportional to the magnetization. Therefore the magnetization can be determined by finding the FMAR. This was done and the results are shown in figure (17). Thus the magnetization curve of the

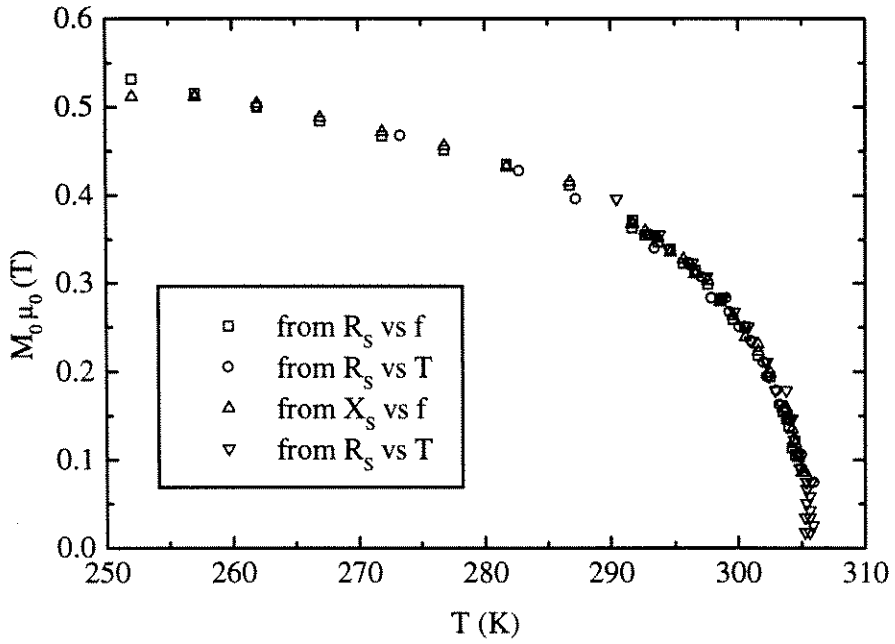

Figure 17: Magnetization data obtained from FMAR from four different dependences.

sample is found without applying any external field, in opposition to the standard magnetometer measurements.

5.2.2 Errors in the Determination of the Magnetization

During the measurement of the frequency dependence of Z_s, the temperature is held constant and measured very accurately, whereas the error in the determined frequency for the FMAR from the frequency dependences is dominated by the width of the features in R_s and X_s. Thus in this case the extracted magnetization will have an error (i.e. an error bar with respect to the magnetization). In the temperature dependence the frequency is set exactly by the network analyzer whereas the temperature is determined as accurately as the features in R_s and X_s

are wide. Thus these magnetization values have an error in temperature. A plot of some of the obtained magnetization values together with their error bars is found in figure (18).

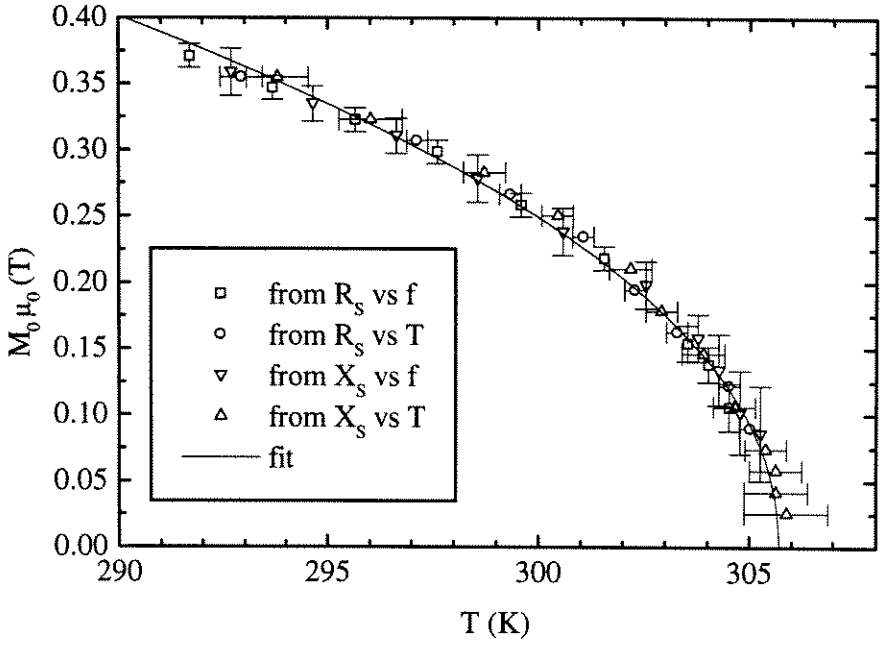

Figure 18: Some of the magnetization data obtained from FMAR with their error bars. The solid line is a fit $\propto (305.7 - \mathrm{T(K)})^{0.47}$

The error in the temperature dependent data becomes larger for higher frequencies, because the magnetization curve flattens out at lower temperatures and therefore the temperature range in which FMAR affects R_s and X_s for the particular frequency broadens.

The error bars in the data from the frequency dependence increase for temperatures closer to T_C: Here R_s and X_s show the strong overall frequency dependence $\sqrt{\omega}$, which covers the FMAR features.

For temperatures close to T_C a new feature occurs in R_s which makes it hard to pinpoint the FMAR minimum. Clearly above T_C the behavior of $La_{0.8}Sr_{0.2}MnO_3$ is like that of a metal without any magnetic effects. Therefore the frequency dependence of R_s is proportional to $\sqrt{\omega}$, which means that for low frequencies R_s

will also be low. Below T_C on the other hand the R_s data takes on a frequency-independent value of $\approx 4\,\Omega$ (compare figure (12)). Thus around T_C for the low frequencies, R_s has to decrease from the value below T_C to that dictated by $\sqrt{\omega}$. Thus a step in R_s occurs in the same temperature range as the FMAR. Thus these two features add and the actual minimum in R_s may not be the temperature where the FMAR condition is fulfilled. In X_s on the other hand there is no such strong enhancement below T_C and therefore the step in X_s remains visible up to temperatures very close to T_C. Thus all the magnetization values very close to T_C were obtained from the temperature dependence of X_s .

5.3 Critical Behavior of Magnetization

5.3.1 Theory

The material under study undergoes a transition from a ferromagnetic state to a paramagnetic state around 305 K. Such a transition is described by the theory of critical behavior [14]. This theory predicts that for the case of zero external field and for temperatures close to the transition temperature, the Curie temperature T_C, the spontaneous magnetization M_0 depends on temperature in the form of a power law:

$$M_0 \propto (T_C - T)^{\beta} \qquad \text{for} \quad T < T_C \tag{32}$$

Here β is the critical exponent. This critical exponent depends on the microscopic mechanism that causes the ferromagnetism, as well as on the dimensionality of the system, but in our case only three-dimensional systems are relevant. Two important theoretical models of magnetism are the mean-field and the Heisenberg models. Mean-field theory assumes that the local environment of the spins in the material are uniform, equivalent to an Hamiltonian assuming interaction of infinitely long range. The mean field prediction of the critical exponent β is 0.5. The 3D Heisenberg model on the other hand assumes only nearest neighbor inter-

action and predicts $\beta = 0.365$ [16]. Therefore the critical exponent is an indicator of the underlying mechanism of magnetism and may give evidence whether the microscopic interaction is short- or long-range.

An absolute determination of β requires very careful measurements. Typically critical behavior is examined by studying the field-dependence of the magnetization, extracting from this the Curie temperature T_C and extrapolating the zero-field magnetization M_0 and then using fitting or other specialized techniques to obtain β [16].

5.3.2 Measured Magnetization Curve

Our experiment allows one to extract the zero-field magnetization directly, without any extrapolation from finite field data. Therefore it might be well suited to extract the critical exponent from our magnetization data.

The direct way to deduce a value of β is to fit our data to the form given by equation (32). In general this is a fit with three fitting parameters: β, T_C and a coefficient for the magnitude of the magnetization. Such fits were performed, but they show a strong dependence on the temperature range over which the fit was applied. Since critical behavior describes the system strictly only for temperatures close to T_C, fit ranges for temperatures close to T_C only should give more accurate results. But then the number of points included in the fit becomes smaller and also the error bars for those values close to T_C are typically large. This complicates the fitting procedure. In my opinion, the most reasonable compromise with respect to the fit range is from 295 K up. Those fits result in $\beta = 0.47$ and $T_C = 305.7\,\mathrm{K}$. The errors for these quantities are given by the range of fits in this temperature range which result in similarly good fits and reveal $\beta = 0.47 \pm 0.04$ and $T_C = (305.7 \pm .5)\,\mathrm{K}$. The value for T_C does not agree with the estimate of 307 K from the SQUID measurement shown in section 4.2. The reason for this

might be that one of the thermometers is not accurately calibrated. The value for β agrees within the error with the mean field theory prediction. Because of the big error, however, this cannot be considered a rigorous proof that mean field theory is the appropriate way to describe the thermodynamics of the magnetism in this material.

Other techniques to extract the critical exponent, like the Kouvel-Fisher method [16], do not help to obtain β more accurately either, since our data is not very smooth and therefore taking the derivative of $M_0(T)$ is problematic.

5.3.3 Comparison with Literature

Since the microscopic mechanism of magnetism in CMR materials is still not completely understood, an exact determination of β would be quite helpful. Studies of different CMR compounds conducted by several groups can be found in the literature [13, 15, 16] and give values of β spanning the whole range from $\beta = 0.3$ to $\beta = 0.5$. For our particular system $La_{0.8}Sr_{0.2}MnO_3$ two values of β were published. One of them [13] was obtained from a single crystal produced in the same way as our present sample. There, several experimental techniques, among them FMAR and FMR, were used to measure values for the magnetization and then the data were fit. The results are $\beta = 0.34 \pm 0.05$ and $T_C = (304 \pm 3)$ K. Thus the T_C determined for these two samples resemble one another, whereas there are large differences in the value for β. The data that were used in the fit in [13] cover the temperature range 270 K - 300 K, a rather wide range, but leaves out a temperature range of the order of 5 K below T_C, which is in fact the only range where the critical behavior should hold. If we fit our data of this temperature range (270 K - 300 K) only, we obtain $\beta = 0.23$ and $T_C = 302$ K, which are clearly off from the more reasonably determined values given above, but deviating from these in the same direction as those given in [13]. This might be an indication that

the fit presented there gives a misleading value.

An in-depth investigation of the critical behavior of $La_{0.8}Sr_{0.2}MnO_3$ from field-dependent magnetization measurements of polycrystalline samples is described in [16]. The results there are $\beta = 0.50 \pm .02$ and $T_C = 315\,K$. Whereas the value for β agrees within error with our result, the values for T_C are different. This difference in T_C might be explained by a small difference in stoichiometry, as the T_C changes rapidly with composition [11].

6 Measurements in Finite Applied Magnetic Field

6.1 Parallel Applied Magnetic Field

The parallel external field was realized by positioning permanent magnets on two sides of the probe, such that the field between the magnets penetrates the sample in a parallel direction. This setup is shown schematically in figure (19). The field strength of the magnetic field can be adjusted by changing the distance

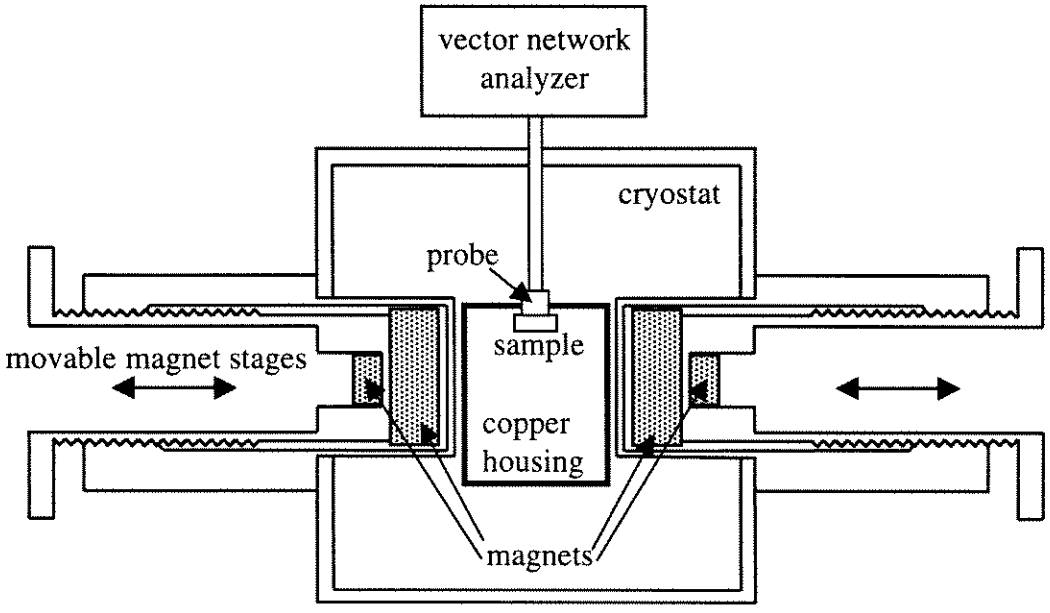

Figure 19: Schematic top view of the setup to create a magnetic field parallel to the sample (not to scale).

between the magnets. Now again the temperature dependence of Z_s for the whole frequency range was measured as well as the dependence on the strength of the magnetic field.

6.1.1 Field Dependence

For finite fields the FMR occurs as a new, strong feature. For the resonance frequencies a maximum in R_s can be seen. The FMAR remains a clear minimum in

R_s. In X_s the resonance gives a sharp decrease, whereas the antiresonance causes a sharp increase. This can be seen for the data shown in figures (20) and (21).

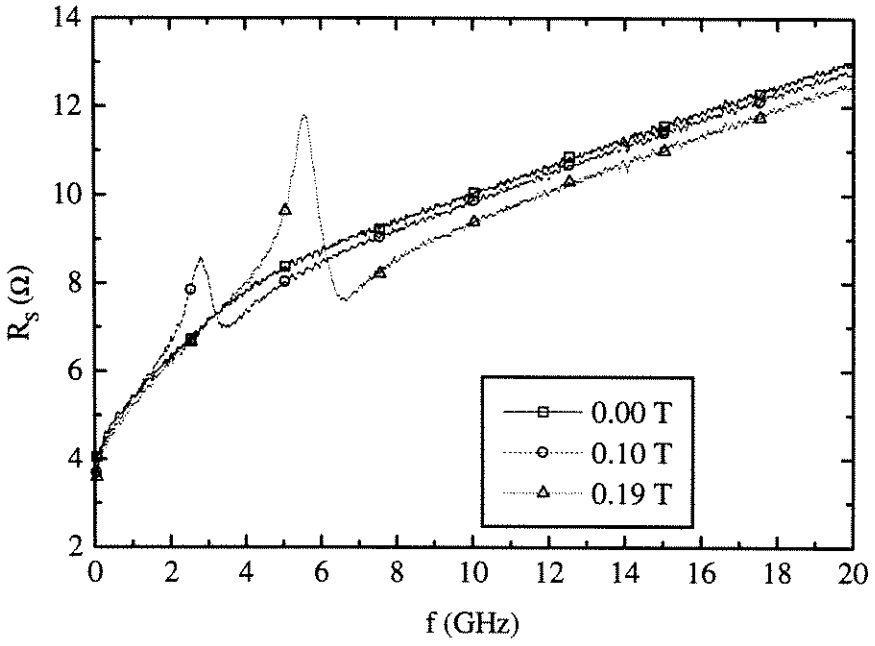

Figure 20: R_s as function of frequency for three different external parallel magnetic fields at 311.4 K

The data in figures (20) and (21) were obtained at a temperature of 311.4 K, well above T_C. Therefore, at least in the case of the high external field, the data should be described by the general model of dynamic susceptibility. The easiest way to check this is to consider the field dependence. The applied external magnetic field of our experiment can be varied in strength by changing the distance between the magnets. Thus the field dependence of Z_s can be measured at a constant temperature. Again for 311.4 K, R_s versus frequency and applied magnetic field is shown in gray scale in figure (22).

Here, as already in the plots of the spectra, the overall $\sqrt{\omega}$ behavior is visible, which is expected since we are above T_C. The resonance is a sharp feature and its frequency seems to increase linearly with applied field. The model predicts for this case $\omega_r = \gamma\sqrt{(N'_y M_0 + H_i)(N'_x M_0 + H_i)}$. Here H_i will be the applied field

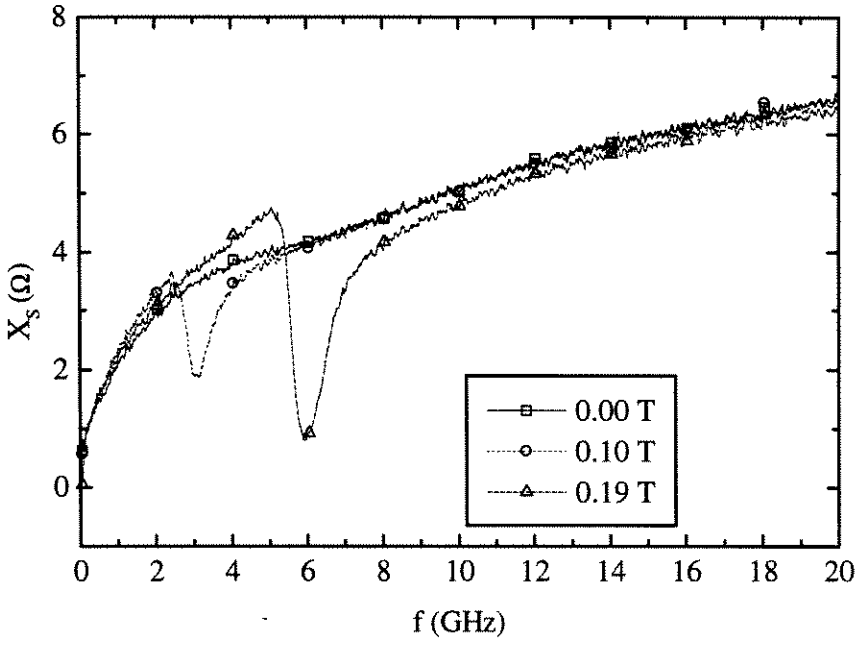

Figure 21: X_s as function of frequency for three different external parallel magnetic fields at 311.4 K

plus the demagnetization field. At this high temperature the magnetization is given by $M_0 = \chi H_i$, where χ is now the static susceptibility. Therefore one has

$$\omega_r = \gamma H_i \sqrt{(N'_y \chi + 1)(N'_x \chi + 1)} \tag{33}$$

In this geometry the demagnetization factor in the direction of the static field is $N_z = 1/8$. As mentioned earlier, the dynamic demagnetization factors are not *a priori* determined. Since the skin depth for our material is of the order of 10 μm at 10 GHz, the effective Corbino disk will be very thin compared to its diameter. Therefore I assume that the dynamic demagnetization in the plane vanishes, whereas the demagnetization factor parallel to the disk is set to one. Then the resonance condition becomes

$$\omega_r = \gamma(1 - \frac{7}{8}\chi)\sqrt{1 + \chi}\, H_0 \tag{34}$$

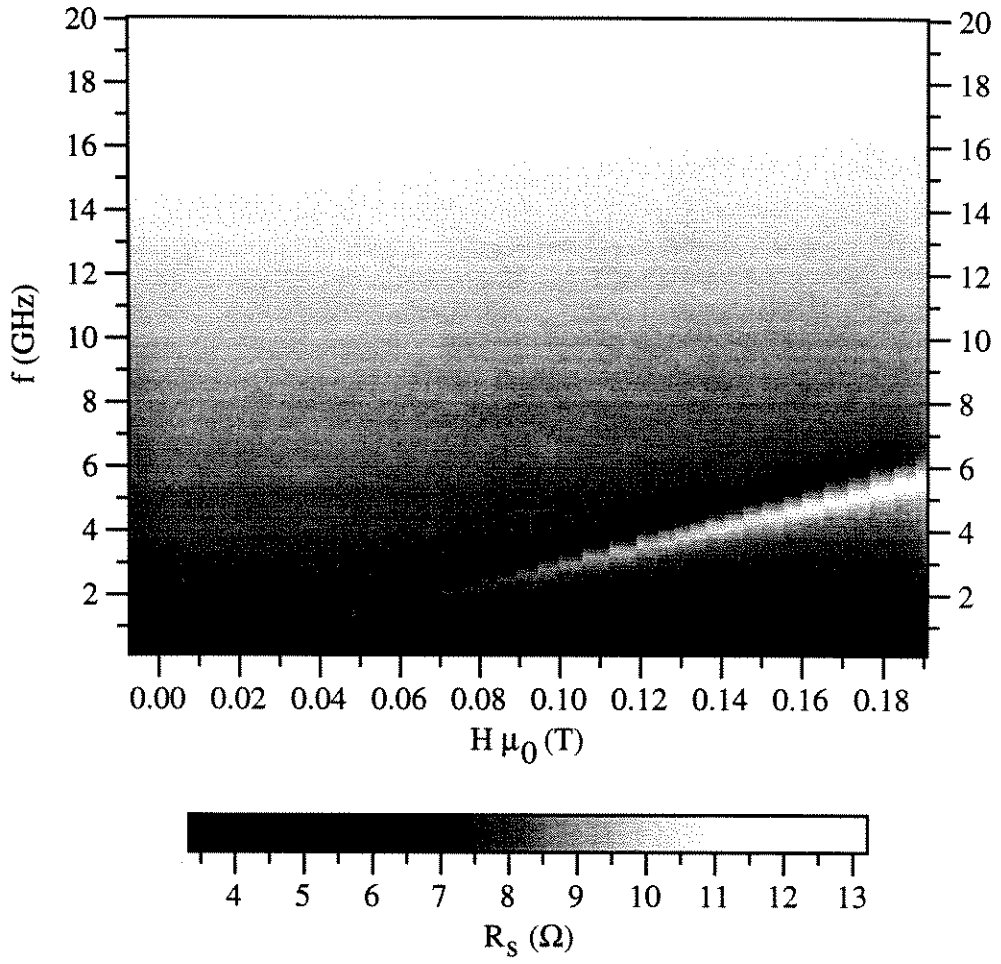

Figure 22: R_s in a gray scale plot as a function of external magnetic field and frequency at 311.4 K. The FMR is the light feature and the FMAR is the dark feature just above the FMR.

Thus the resonance frequency increases linearly with the applied field. The same is true for the antiresonance:

$$\omega_{ar} = \gamma(1 - \frac{7}{8}\chi)(1 + \chi)H_0 \tag{35}$$

For temperatures well below T_C the situation is quite different. For 276.6 K the field and frequency dependence of R_s is shown in gray scale in figure (23). The resonance does not seem to be directly proportional to H any more. For an applied field higher than 0.055 T the resonance frequency seems to increase linearly with

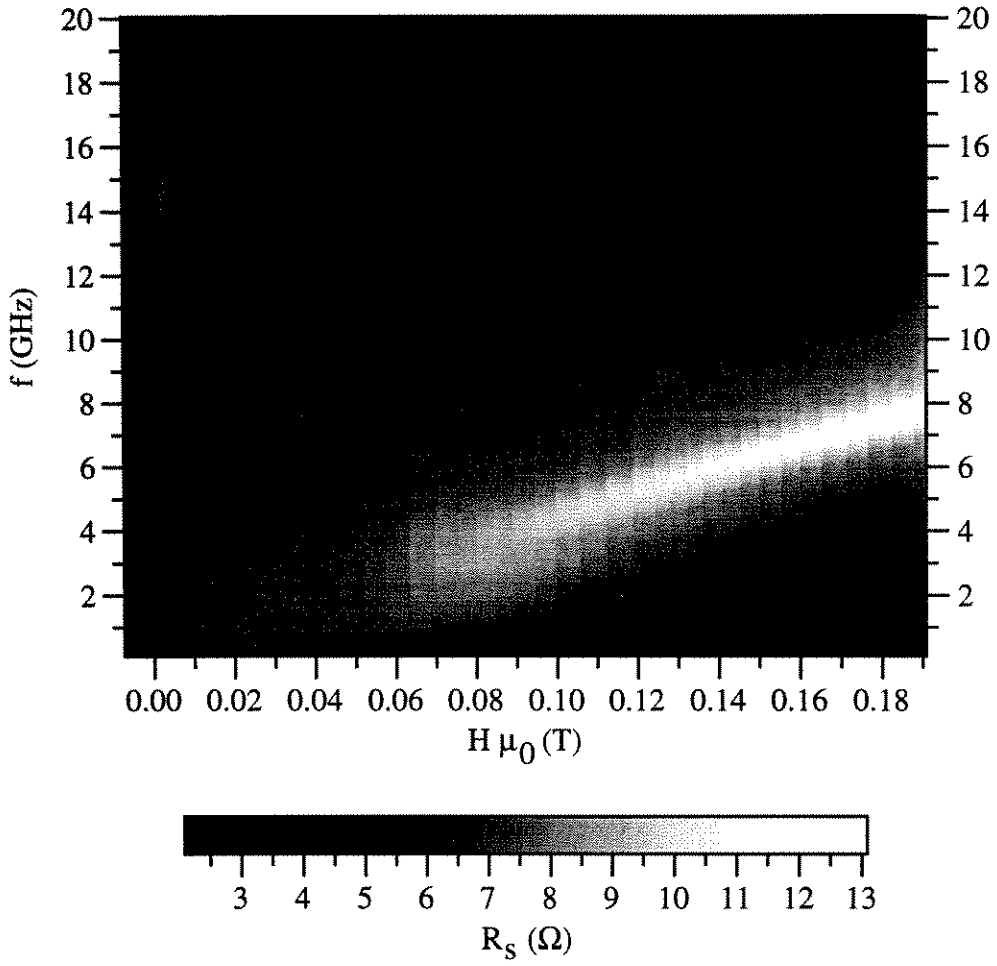

Figure 23: R_s in a gray scale plot as a function of external magnetic field and frequency at 276.6 K. The dark feature across the top is the FMAR, the light feature is the FMR.

the field, but below 0.055 T the resonance weakens considerably. Examination of the single spectra shows that below 0.055 T a maximum in R_s still exists, but it is very weak and field independent around 2.5 GHz. The antiresonance is well separated from the resonance. Above 0.055 T the FMAR frequency also increases linearly with field and below 0.055 T it is constant at 12.85 GHz. Thus a remarkable feature is that FMR and FMAR seem to be field independent below 0.055 T. I denote this particular field as $H_=$ and the according magnetization as $M_=$.

The field independence of ω_r and ω_{ar} below $H_=$ can be explained by con-

sidering the static demagnetization field. At $H_=$ the demagnetization is saturated, corresponding to a uniform magnetization. This means that the applied and demagnetization fields are equal. With the static demagnetization factor $N_z = 1/8$ this gives $H_= = (1/8)\,M_0$. Since $H_= = 0.055\,T/\mu_0$ this reveals $M_= = 0.44\,T/\mu_0$, corresponding to a frequency of 12.3 GHz. Below 0.055 T the applied magnetic field always induces a static demagnetization field that inside the sample exactly cancels the external field. Therefore for the low fields there are no differences in FMR and FMAR compared to the zero field measurement.

The antiresonance according to Eq.(31), again assuming $N'_y = 1$ and $N'_x = 0$ is predicted to be at

$$\omega_{ar} = \gamma(H_i + M_0) \tag{36}$$

If there was indeed no magnetic field inside the sample, $H_i = 0$, the antiresonance should occur at 12.3 GHz. The experiment on the other hand gives 12.8 GHz as the FMAR frequency. According to Eq.(36) this means that in fact there is a magnetic field present, corresponding to 0.5 GHz or 0.017 T. This field is caused by anisotropy in the magnetization and other imperfections of the sample and will not be uniform. This generic internal field H′ will have different directions and different strengths for different places in the sample, but the average will be around 0.017 T. The presence of this internal field is essential for the model. If there was exactly zero field inside the sample, there would be no precession of the magnetization and thus the model would not apply.

Since there is a magnetic field, there should be a resonance. From Eq. (30) with the same assumptions as above one gets

$$\omega_r = \gamma\sqrt{H_i(H_i + M_0)}. \tag{37}$$

With $H_i = H' = 0.017\,T/\mu_0$ this gives $\omega_r = 2.5$ GHz, exactly where the weak maximum in R_s for the low fields can be found.

Above $H_=$ the internal magnetic field gets additional components from the external field, which starts penetrating. Since the direction of H' will be not uniform within the sample, for $H_i \gg H'$ the FMAR frequency will increase linearly with the external field and the average internal field will be $H_i = H_0 - N_z M_0$, where $N_z = 1/8$ is the static demagnetization factor. Thus for $H_0 > H_=$ the FMAR condition becomes

$$\omega_{ar} = \gamma(\frac{7}{8}M_0 + H_0) \tag{38}$$

and the slope of the FMAR frequency f_{ar} should be $\gamma/(2\pi) = 28$ GHz/T. A fit of the experimental values of f_{ar} vs. H_0 for $H > H_=$ gives a slope of 29 GHz/T.

The condition (37) for FMR might also be applied in the same way for $H > H_=$. But since not the external, but the effective internal field enters as a factor, the external field will dominate the resonance frequency only when H_0 is considerably higher than $H_=$. However, if ω_r is calculated with $H_i = H_0 - (1/8)M_0$, the result agrees with the experimental data for the higher fields that were measured. This is shown in figure (24).

For external fields only slightly above $H_=$ the effective internal field gradually increases as the part of the external field that penetrates the sample increases, such that a gradual transition from the constant FMR frequency for low fields to the curve described by Eq. (37), as seen in the data, can be expected.

With our discussion of the data at 276.6 K and 311.4 K, two temperatures have been examined that are well below and well above T_C. For temperatures around T_C a gradual transition from the case with a low field, field independent region to those with clear linear field dependences of FMR and FMAR frequencies takes place.

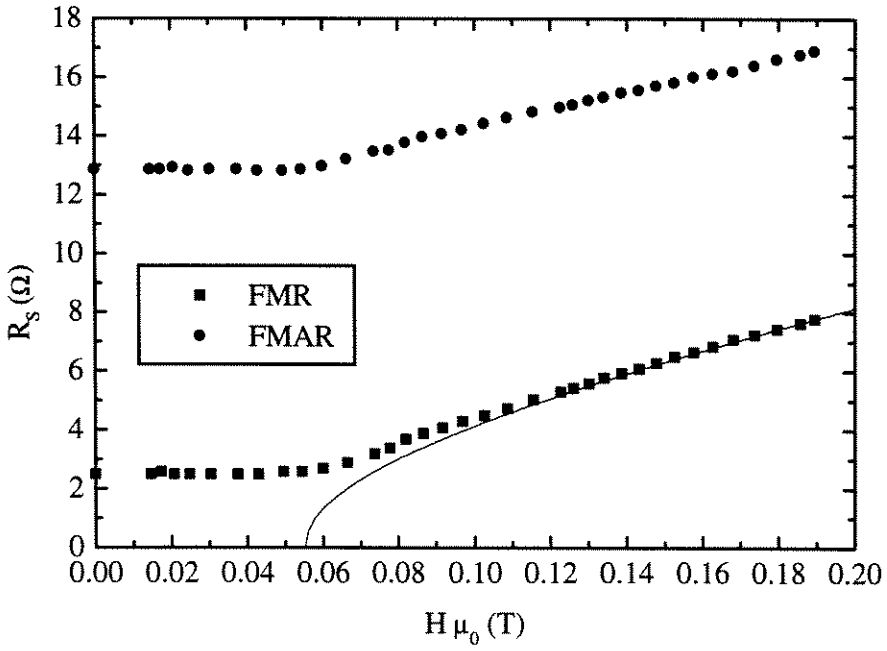

Figure 24: FMR and FMAR frequencies as a function of external field for 276.6 K. The solid line is a calculation of the FMR frequency based on the external magnetic field that penetrates the sample, neglecting the intrinsic internal field.

6.1.2 Temperature Dependence

Now that the field dependence of the FMR and FMAR frequencies seems to be understood, they may also be investigated as a function of temperature at a fixed field. The spectra of R_s and X_s in the highest accessible parallel field of 0.19 T for different temperatures are shown in figures (25) and (26).

As seen in the previous section, FMR and FMAR are sharp features for this applied field. To demonstrate the temperature dependence of the FMR and FMAR frequencies another gray scale plot is presented in figure (27).

Here the antiresonance is the dark band as was already seen in the similar plot for zero applied field. As described in the previous section about the field dependence, at 276.6 K (the lowest temperatures measured in these experiments), an applied field of 0.055 T saturates the demagnetization. Therefore in an applied field of 0.19 T as in this case the FMR and FMAR frequencies will be determined

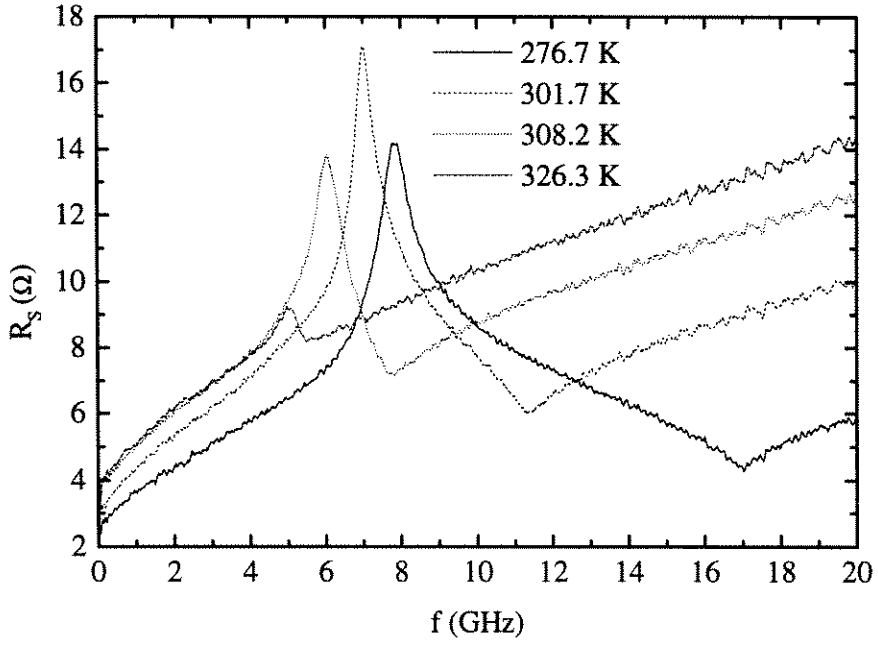

Figure 25: R_s as a function of frequency for the $La_{0.8}Sr_{0.2}MnO_3$ single crystal in an external field of 0.19 T

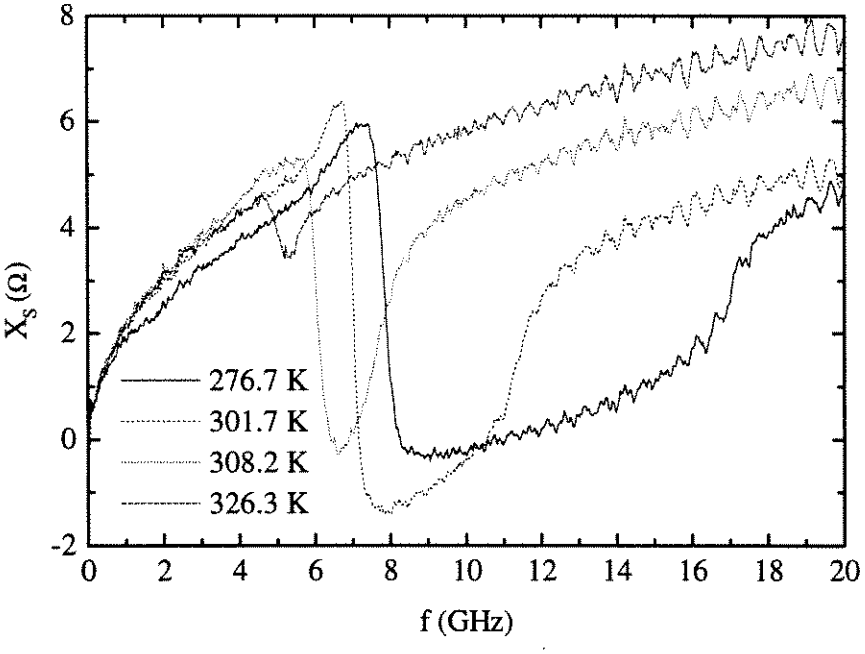

Figure 26: X_s as a function of frequency for the $La_{0.8}Sr_{0.2}MnO_3$ single crystal in an external field of 0.19 T

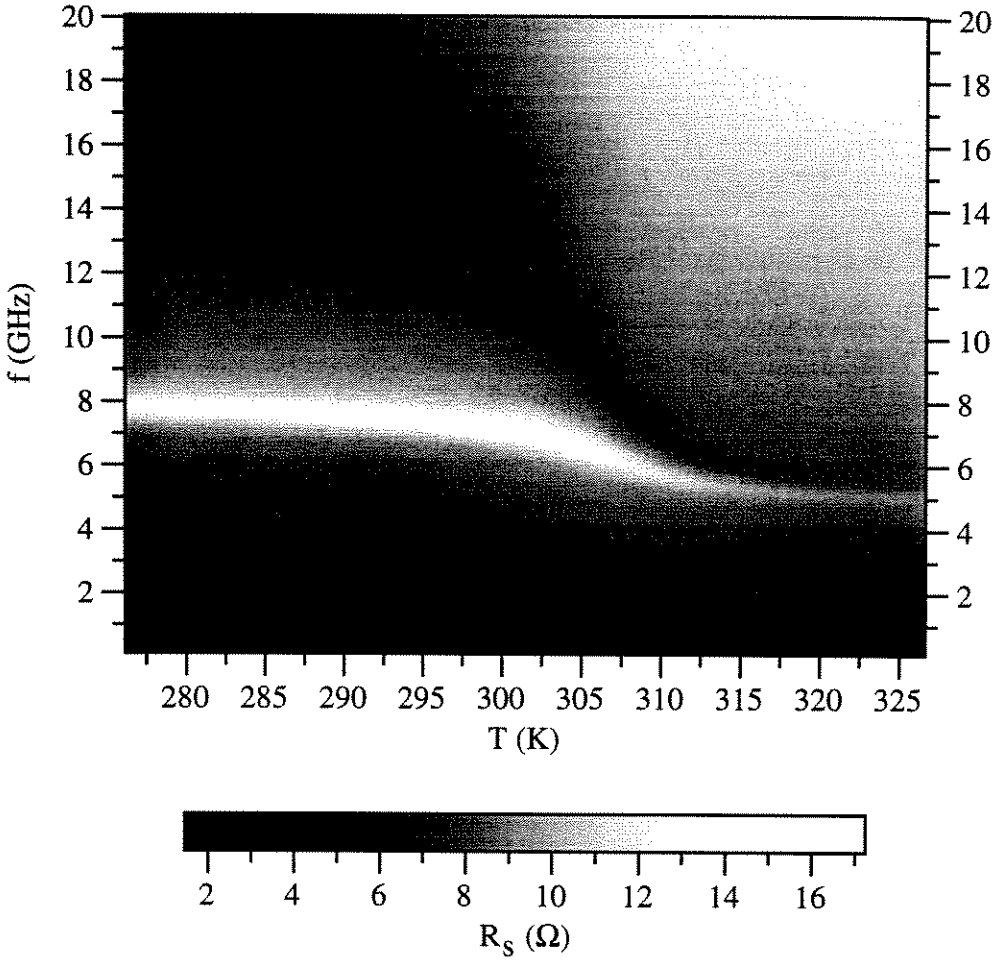

Figure 27: R_s in a gray scale plot as a function of temperature and frequency for an applied external magnetic field of 0.19 T parallel to the sample

by the external field for all temperatures above 276.6 K. As seen before, in this regime the conditions for FMR and FMAR become:

$$\omega_r = \gamma\sqrt{H_i(H_i + M_0)} = \gamma\sqrt{(H_0 - \frac{1}{8}M_0)(H_0 + \frac{7}{8}M_0)} \tag{39}$$

$$\omega_{ar} = \gamma(H_i + M_0) = \gamma(H_0 + \frac{7}{8}M_0) \tag{40}$$

Since the external field H_0 is held constant, it is easy to determine the magnetization from the position of the antiresonance. The resulting magnetization curve is shown in figure (28), together with the data from the SQUID measurement with an applied parallel magnetic field H=0.2 T/μ_0. Here the two magnetization curves,

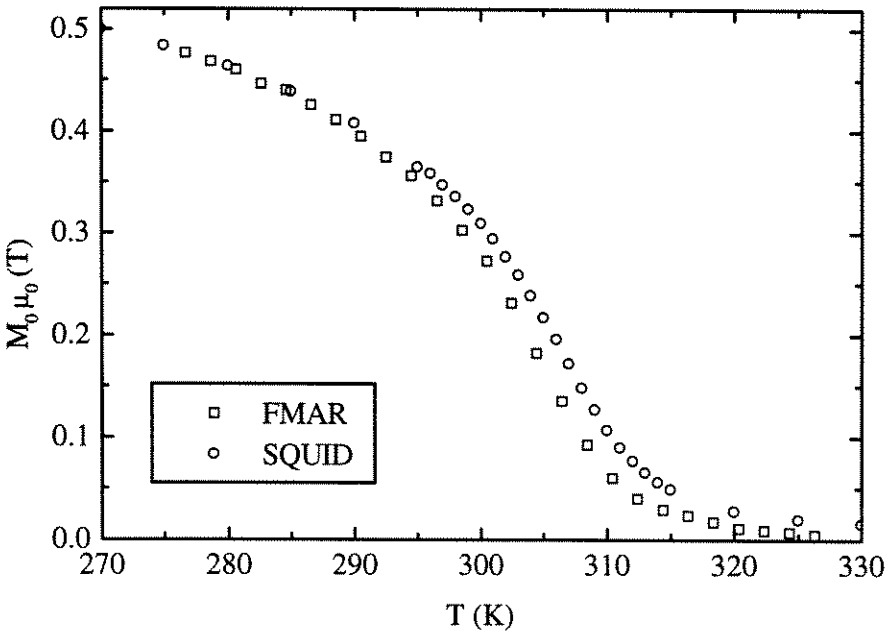

Figure 28: The magnetization for an applied field of 0.19 T parallel to the disk obtained from FMAR compared to the magnetization measured with a SQUID at an applied parallel field of 0.2 T.

obtained from completely independent measurements, do not only agree qualitatively with each other, but also quantitatively. The only difference is an apparent shift of one of the curves about 1 K in temperature with respect to the other. This may be due to insufficient calibration of one of the thermometers. This would be consistent with the estimation of T_C from the SQUID measurement, which was also slightly higher than the value deduced from the FMAR data. Thus the resonance and antiresonance frequencies can be described well using a modified version of the model described in chapter 3.

One of the results is that in the case of a small applied field parallel to the disk ($H_0 < H_=$) the antiresonance can be found at $\omega_{ar} = \gamma(H' + M_0)$, which also holds for the zero field case. In chapter 5 on the other hand $\omega_{ar} = \gamma M_0$ was assumed. Now this turns out to be not quite correct, since the internal fields were neglected. One reason for this procedure is that there is no direct way to determine

H′. In the case above, H′ can be estimated because the frequency dependence of the resonance can be followed from the sharp peak at high fields to the weak maximum for the zero field case. If only zero field data is available, it is hard to reliably determine the resonance frequency. Furthermore H′ can be assumed to be related to the spontaneous magnetization. If the determined and the real spontaneous magnetization only differ by a factor (1.04 in the above case) the temperature dependence will not be affected.

6.1.3 Resonance Linewidth

From the field dependence measurements the resonance linewidth can be extracted. Unfortunately the step width between the different fields that were measured are around 0.005 T/μ_0, whereas the observed FMR line width is of the order of 0.03 T/μ_0. Thus the field resolution is not adequate to determine precise values of the linewidth, but general observations are possible. But since we also obtain the frequency dependence, we can also determine the line width in frequencies. Whereas the determination of the line width from the field dependence is a standard for most of the FMR investigations, most of the experiments cannot observe the linewidth in the frequency dependence, since they are bound to specific resonant frequencies.

In the region where the resonance is well defined the linewidth from the field dependence is frequency independent. Furthermore the linewidths in frequency and those in field are proportional, the proportionality factor is γ. The temperature dependence of the linewidth is shown in figure (29). The linewidth is generally of the order of 0.03 T/μ_0 and decreases slightly with increasing temperature. For a similar $La_{0.8}Sr_{0.2}MnO_3$ single crystal an increase of the linewidth (from 0.01 T/μ_0 to 0.0175 T/μ_0) around T_C was reported [13] and attributed to a spread in T_C within the sample [17]. Unfortunately our resolution is insufficient to conclusively

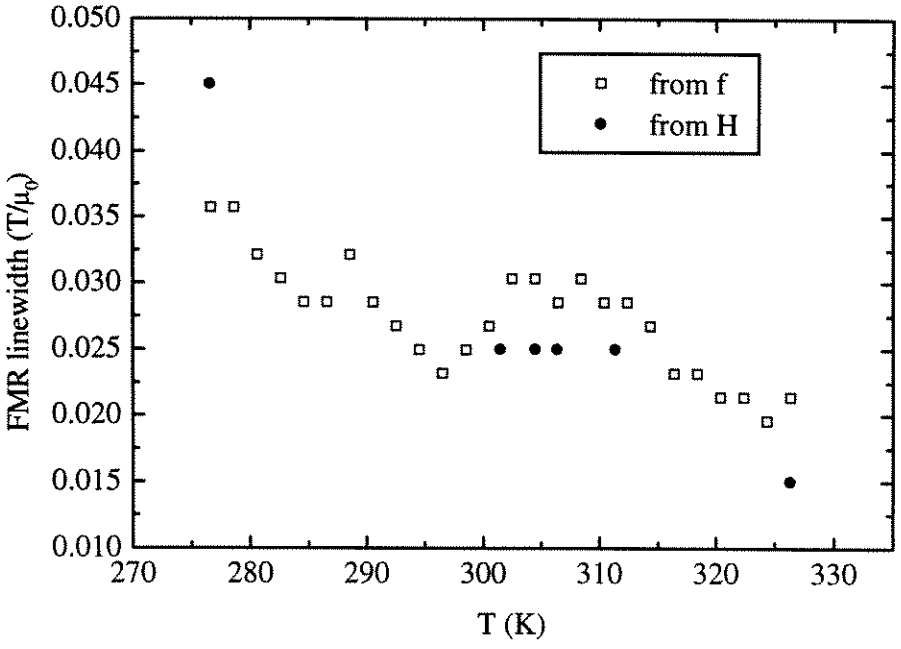

Figure 29: FMR linewidth in the field dependence as well as in the frequency dependence for the parallel field case.

state whether there is an increase in the linewidth around T_C, if there is one, it is by less than 0.005 T/μ_0.

It should be noted that the linewidth is of the order of the estimate 0.017 T/μ_0 for the generic internal field. Since this internal field will influence the resonance frequency, the linewidth should at least be as big as this nonuniform internal field.

6.2 Perpendicular Applied Field

6.2.1 Temperature Dependence

Measurements with a magnetic field perpendicular to the disk were performed by placing a permanent magnet into the copper barrel between the sample and the supporting copper pedestal. This is schematically shown in figure (30). The magnet, which has a diameter only slightly smaller than the inner diameter

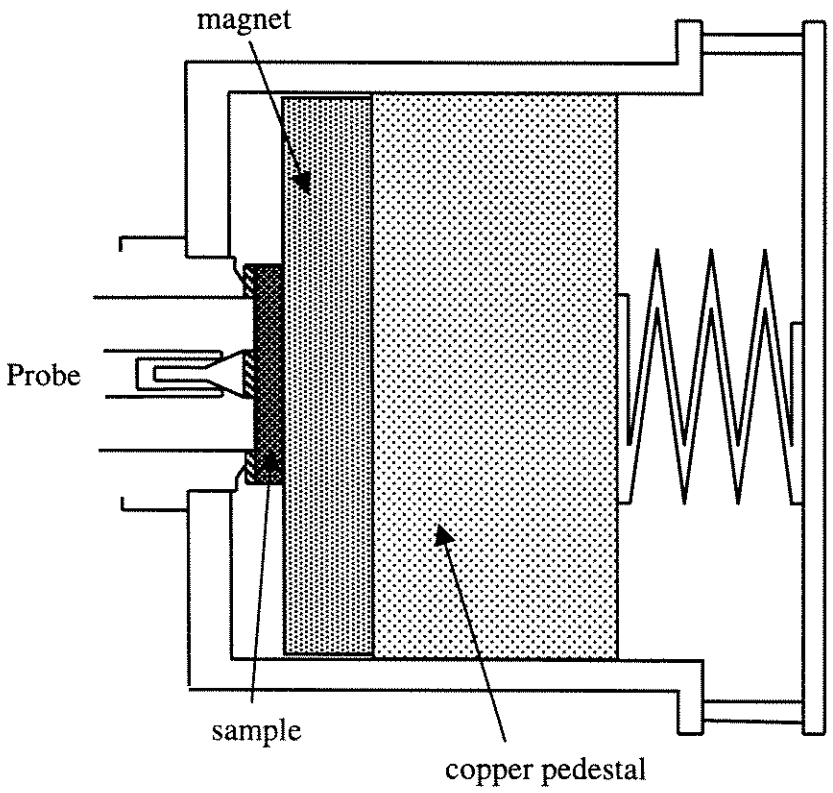

Figure 30: Schematic view of the mounting of the magnet to create a magnetic field perpendicular to the sample (not to scale).

of the copper housing that surrounds the probe, is fixed on top of the copper pedestal that is used to press the sample against the probe connector. The sample is then placed directly on the magnet. The diameter of the sample of 3.9 mm is much smaller than the diameter of the magnet of about 10 mm. Since the sample is about 0.8 mm thick, the field inside the sample can be assumed to be almost uniform, but the magnetic field on top of the sample will be somewhat smaller than directly on top of the magnet. Two different magnets were used, their field strengths at the surface are 0.25 T and 0.38 T respectively.

For these two fields Z_s was again measured as a function of frequency and temperature. The results for the 0.25 T magnet are shown in a gray scale plot in figure (31). Again the resonance is seen as a sharp feature for temperatures above 302 K. But in opposition to the parallel field case, the resonance frequency

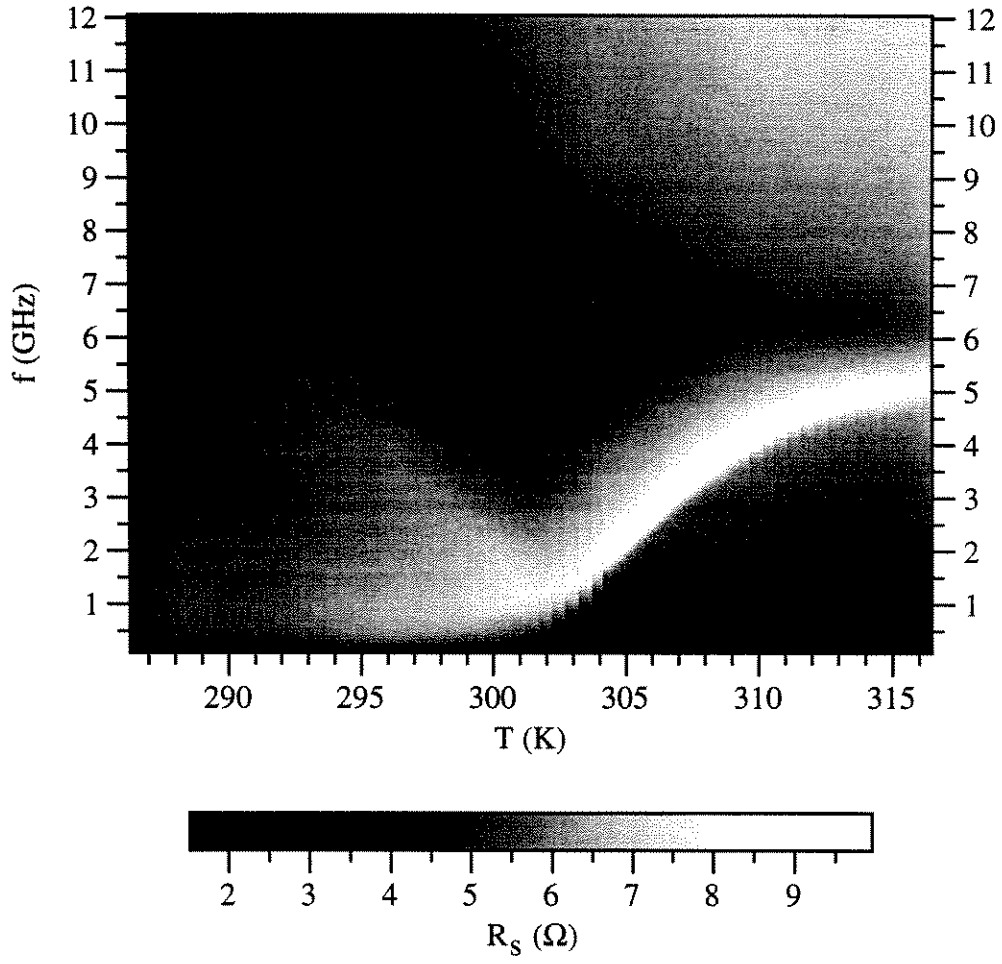

Figure 31: R_s in a gray scale plot as a function of temperature and frequency for an applied perpendicular field of 0.25 T

increases with temperature in this range. Below 302 K the resonance seems to split into two maxima, one almost constant in frequency around 1 GHz, the other one increasing in frequency for decreasing temperature. The antiresonance can be found throughout the whole observed temperature range, but broadens considerably around 302 K. Unfortunately a conclusive interpretation of all of the effects remains still to be found. However, some parts can be interpreted in the picture conveyed in the previous section.

First the static demagnetization factor should be considered. Since now the disk is perpendicular to the applied field, the demagnetization factor is 3/4

in the direction of the field. This means that a much bigger fraction of the magnetization contributes to the demagnetization field and therefore the applied field will be effectively screened from the inside at a considerably lower magnetization than in the parallel case. The theoretical FMR and FMAR frequencies for the perpendicular field case (assuming that the dynamic demagnetization factors are $N'_x = N'_y = 0$) are:

$$\omega_{ar} = \gamma |H_i| \tag{41}$$

$$\omega_r = \gamma \sqrt{(M_0 + H_i)H_i} \tag{42}$$

Thus the resonance seems to be easily predictable. For high temperatures the magnetization will be small and therefore the applied field will magnetize the sample uniformly. There $H_i = H_0 - 3/4\, M_0$ should hold. For the highest temperatures the magnetization will be very small compared to the applied field and then $H_i \approx H_0$. In this case the FMR and FMAR frequencies both are γH_0. At 316 K the FMR frequency is 5.1 GHz, the FMAR frequency is 6.4 GHz. Thus the effective applied magnetic field will be about 0.22 T/μ_0.

At some temperature the magnetization will be big enough to cause a demagnetization field that compensates the applied field inside the sample. Below this temperature the internal field should be only the intrinsic H' and should therefore not change too much with temperature. This temperature dependence seems to be exactly what can be found for the FMR in the experiment for temperatures higher than 302: With increasing temperature the magnetization decreases, therefore the demagnetization field becomes smaller and thus the internal field becomes larger (since the external field is held constant). Below 302 K the lower of the two maxima also seems to fit the prediction: its frequency is almost temperature independent, corresponding to the intrinsic H'. Thus this resonance can be explained if the model is applied in the same fashion as before.

If the antiresonance is considered, the interpretation is less straightforward. For the lowest temperatures the FMAR frequency occurs at exactly the same frequencies as in the zero field case. For those temperatures the magnetization in zero field is considerably larger than the now applied field. Therefore the local magnetization in zero and finite field will not differ too much for these temperatures. The position of the antiresonance thus suggests that the FMAR frequency is given by $\omega_{ar} = \gamma(H' + M_0)$. But this is the relation for the parallel applied field. This may be explained by the following: For these temperatures the demagnetization field is strong enough to effectively compensate for the applied field and the internal field is only H'. But as mentioned earlier, the direction of H' is not uniform. Therefore it should not matter whether the external field is parallel or perpendicular, since it does not affect the internal field anyway. Thus the position of the FMAR should be the same for both cases. The fact that the system seems to act as if H' was parallel to the disk may be a hint that the spontaneous magnetization prefers to be in the plane of the sample. If this was true, also a resonance caused by H' should be found at the same frequency as in the zero field case, around 2 GHz. But the perpendicular field data does not show a maximum at this particular frequency. For temperatures above 308 K the antiresonance frequency is almost temperature independent, the variation with temperature is much less than that of the resonance in this region. This is more consistent with the antiresonance condition for the perpendicular case, $\omega_{ar} = \gamma\sqrt{(M_0 + H_i)H_i}$, than the one for the parallel case. Thus the antiresonance seems to follow the condition for the perpendicular field for high temperatures, where the magnetization is expected to be uniform and parallel to the applied field, but for lower temperatures it changes to the case of no internal field except for H' and the FMAR frequency is determined by the relation for the parallel case.

The second maximum below 302 K seems to be at the frequency determined by $\omega = \gamma(M_0 - H_0)$, but there is no theoretical support for this. The temperature 302 K is the temperature at which the demagnetization field cancels the external field. But neither the external field nor the magnetization are know exactly. Furthermore the magnetic field inside the sample varies with the distance from the magnet. Therefore the demagnetization field cannot be considered uniform either, complicating an estimate of the temperature at which the demagnetization field should cancel the applied field.

The data obtained with the 0.38 T magnet look similar, and seem to follow the same behavior as described for the 0.25 T magnet. But since the applied field is stronger, the temperature at which the two different maxima start to evolve, is much lower, around 290 K.

6.2.2 Linewidth

As in the case of the parallel field, the FMR linewidth can be extracted from the frequency spectra of Z_s. The temperature dependence of the linewidth converted to magnetic fields is shown in figure (32).

Again an overall decrease of the linewidth with temperature is observed. Additionally in the 0.25 T case a sharp maximum in the linewidth occurs around 300 K. The reason for this is that at this temperature the two different maxima in R_s, which are present at lower temperatures, meet. Therefore the two cannot be separated and the linewidth indicated is a combined linewidth of the two. At some temperature the two can be separated and therefore the FMR linewidth becomes much smaller again. Thus this maximum in the linewidth has no connection to a spread in T_C as discussed in the case of the parallel applied field, but is caused by the second maximum.

The same occurs for the 0.38 T case, but in the measured temperature range

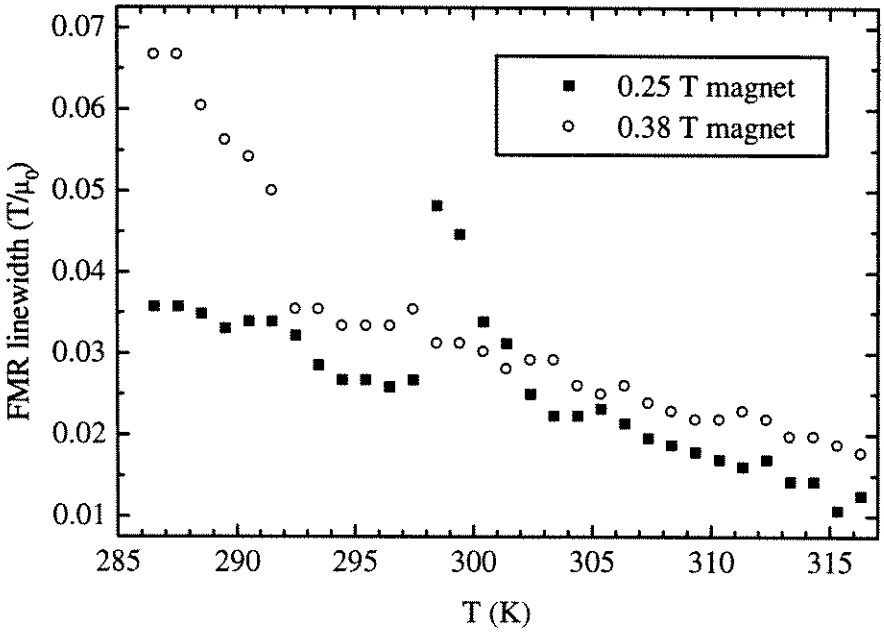

Figure 32: FMR linewidth obtained from the frequency dependence for the perpendicular field of two different magnets.

the two different branches are not seen yet, because $T_=$ is lower than in the case of the lower field.

7 Evaluation of the Quantitative Surface Impedance

The main purpose of our Corbino experiment is to measure the surface impedance Z_s quantitatively. Our setup and the calibration procedure described in chapter 2 should make this goal realizable. However, in our measurements the obtained absolute values for Z_s show some discrepancies when compared to the expected behavior and also some effects that are not completely reproducible. These problems will be discussed in this section, but it should be mentioned that these problems will not affect the results about FMR and FMAR stated above, since they are strong features in our measurements and do not rely on quantitative values of the Z_s, but only on the relative change as a function of the parameters frequency, temperature and magnetic field.

The theoretical prediction for the surface impedance is given by $Z_s = \sqrt{i\omega\mu\rho}$. This implies, that in the limit $\omega \rightarrow 0$, Z_s should also go to zero (since μ and ρ do not diverge for $\omega \rightarrow 0$). This is not what we see in our measurements. Whereas X_s often approaches zero for ω going to zero, R_s usually seems to approach a constant non-zero value, typically around 4 Ω. Whereas X_s does not show this considerable offset, the frequency dependence does not always correspond to the expected $\sqrt{\omega}$ behavior either. It seems as if the frequency spectra of X_s were tilted. This tilt strongly depends on the temperature dependent data correction. In one case where background measurements were performed before and after sample measurements, therefore separated by several days, the corrected Z_s data showed differences between the two corrections. Whereas the R_s data were shifted by approximately 0.3 Ω, the $X_s(\omega)$-data was tilted considerably.

Another supporting argument for the classification of the R_s offset and the X_s tilt as an experimental artefact is, that after a subtraction of the tilt and the

offset the spectra obtained for the $La_{0.8}Sr_{0.2}MnO_3$ sample at high temperatures, clearly above T_C, fit well to the $\sqrt{\omega}$ expectations.

A tilt in X_s may be explained by changes in the transmission line. If the physical properties of the coaxial cable change, e.g. the speed and thus the wavelength of the electromagnetic waves in the transmission line due to changes of the dielectric constant or the total length of the line due to thermal expansion, the phase offset caused by the line will change, where the change is proportional to the frequency. If there are differences between the calibration, the background measurement and the sample measurement, our data correction procedure will attribute this to the surface impedance. Changes of the room temperature may be a reason for changes in the transmission line and thus for the observed tilt in X_s. R_s on the other hand will be less affected by small physical changes of the transmission line, since the attenuation should not change significantly within the temperature range of the measurements.

Another possible origin of the offset might be a misalignment of the probe connector and the Corbino disk. The alignment cannot be checked *in situ*. The sample is fixed and aligned to the center of the copper pedestal before it is inserted into the copper housing. If all these elements are concentric, then the alignment works out, but there is no way to check the alignment. Experiments performed with a scanning near-field microwave microscope on $La_{0.7}Ca_{0.3}MnO_3$ thin films suggest that an inaccurate alignment may also effect the measured surface impedance, but only a weak effect was seen for the $La_{0.8}Sr_{0.2}MnO_3$ single crystal. (These experiments are described in the appendix.)

One drawback originating from the offset and the tilt is, that it is not possible to calculate $\mu(\omega)$ from the data directly. As mentioned above, surface impedance and permeability are related by $Z_s = \sqrt{i\omega\mu\rho}$. That means, if Z_s is known, as is ρ, which in our case we assume to be real and the dc value, then $\mu(\omega)$

can be calculated. However, since our data for Z_s does not vanish for $\omega \rightarrow 0$, the above formula will result in diverging values for μ in this limit, which are obviously unphysical. This problem can only partially be solved by subtracting an offset and a tilt. These problems prevent an access to μ, which would be the primary quantity to consider not only for the intrinsic resonance effects, but also for investigation of critical behavior.

8 Conclusions and Future Work

The Corbino apparatus has proven to be a powerful instrument to investigate the complex microwave surface impedance of a $La_{0.8}Sr_{0.2}MnO_3$ single crystal in general and to observe ferromagnetic resonance and antiresonance in particular. The complete temperature dependence of these phenomena has been obtained and also the influence of external fields was determined. In opposition to the more common resonance experiments, the complete frequency dependence was obtained. This simplified the interpretation of the data, since the continuous change of the FMR and FMAR frequencies with respect to temperature and applied field could be followed. Especially the cases of low magnetic field and magnetizations, corresponding to low frequencies, can be studied much more intensively with our broadband experiment than with resonant techniques. Here the observation the of zero field antiresonance was used to examine the spontaneous magnetization.

Up to now only one single crystal sample has been measured extensively. Another sample should be measured to confirm the general results. If the sample thickness can be chosen to be different than the present one, the static demagnetization factors will be different. That gives the chance to check the conditions of the FMR and FMAR frequencies that depend on the demagnetization factors.

In our current setup it is not possible to continuously change the magnetic field perpendicular to the disk and unfortunately an implementation of a variable perpendicular field requires a new design of the experiment. This is even more unfortunate since the data obtained in perpendicular field are certainly not completely understood yet, the observed temperature dependence of the FMAR in this case seems to be without any relation to the model of the dynamic susceptibility that could explain the FMR and FMAR frequencies for the other measurements in a satisfying manner.

A different limitation of the current setup is the highest obtainable tem-

perature of about 325 K. This range could be extended with a reasonable effort and this would allow the observation of other compounds with a higher T_C such as $La_{0.7}Sr_{0.3}MnO_3$.

Another possible subject are thin films of CMR compounds, preliminary measurements of $La_{0.7}Ca_{0.3}MnO_3$ and $La_{0.7}Sr_{0.3}MnO_3$ thin films have already been performed. But in these cases the substrate of the films dominates the measured surface impedance and therefore the data has to be subject of a much more complicated procedure to disentangle the effects of the thin film and the substrate.

Another flaw in the current experiment is the fact that the measured surface resistance seems to have an offset, it does not vanish for low frequencies. In spite of an intensive search the origin of this offset is still unknown. If this problem could be solved, an extraction of the frequency dependent permeability would be possible and therefore a possibly better approach to observe critical behavior.

Appendix: Investigations Using a Scanning Near-Field Microwave Microscope

One possible reason for our problems in obtaining the surface impedance quantitatively in the Corbino experiment, that were discussed in chapter 7, is a misalignment of the probe and the gold contacts of the sample. Since the alignment cannot be checked or changed *in situ*, a different approach to examine the effects of misalignment was tried.

The $La_{0.8}Sr_{0.2}MnO_3$ sample was examined using a scanning near-field microwave microscope [18]. The microscope probe, an open-ended piece of 0.086-inch diameter coaxial cable, is generally of the same form as the Corbino probe, but its diameter is smaller and it does not operate in contact with the sample, but of the order of 50 to 100 μm above it. Nevertheless, moving the sample with respect to the microscope probe may show the same effect as changing the alignment of the Corbino experiment.

The microscope probe is part of a resonant circuit. As the sample is moved under the probe, the frequency shift of the resonant circuit and the 2f signal, which reflects the quality factor of the resonator, are measured. The frequency shift and the 2f signal, measured across the diameter of the $La_{0.8}Sr_{0.2}MnO_3$ single crystal, are shown in figure (33).

In both, frequency shift and 2f signal, the sample with its diameter of 3.8 mm is visible. The frequency shift is smaller above the sample than away from it. This is consistent with the idea that the sample modifies the open-ended probe towards a shorted end. But besides this overall effect the frequency shift does not show unambiguous features. The shape of the curve above the sample with a minimum in its center may be due to topography, the sample is probably slightly higher in the center than at its edges. The 2f signal does not reveal more

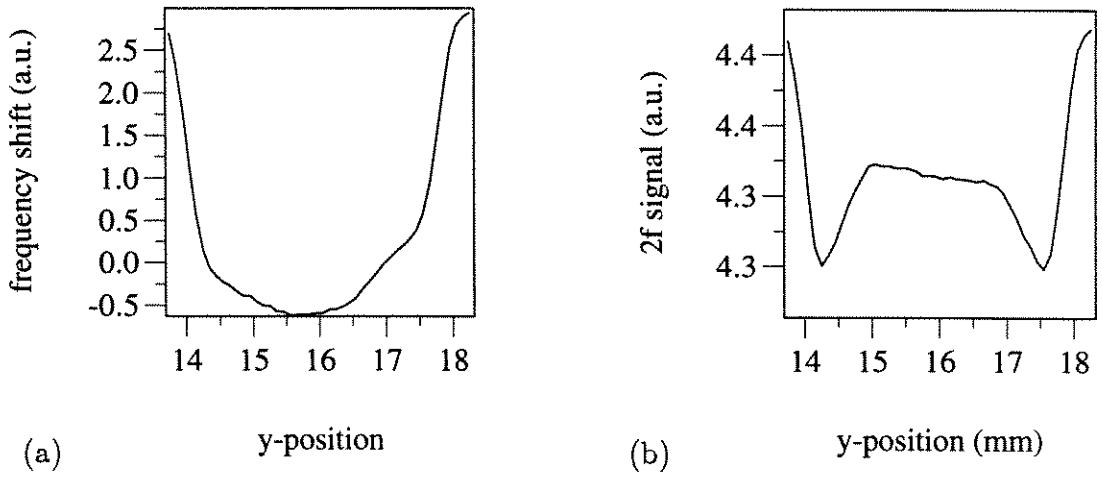

Figure 33: Position dependence of (a) frequency shift and (b) 2f signal for the $La_{0.8}Sr_{0.2}MnO_3$ single crystal

information either. Generally the Q above the sample is lower than away from the sample, but the two sharp minima in the 2f signal may be an edge effect.

A $La_{0.7}Ca_{0.3}MnO_3$ thin film sample was also examined with the microscope. This sample has the same Corbino disk size, but since its overall size is much bigger (roughly a square with the sides 6.5 mm long), the outer gold contact is also larger. Therefore the Corbino disk itself can now be observed without edge effects of the sample. Also this sample does not have the problem of a curved surface. Furthermore the sheet resistance of the thin film is much larger than that of the single crystal and therefore the contrast between sample and gold contacts is bigger. Frequency shift and 2f signal along a diameter of the Corbino disk are shown in figure (34). Figure (35) shows gray scale plots of these two quantities as a function of position over the whole Corbino disk. (The actual shape of the gold contacts can be found in figure (8).)

Here the scan range is smaller than for the $La_{0.8}Sr_{0.2}MnO_3$ single crystal, only the region around the Corbino disk was examined. Therefore the region outside the disk is the gold contact, which acts more like a short than the $La_{0.7}Ca_{0.3}MnO_3$ disk. Thus the frequency shift increases above the disk, since it

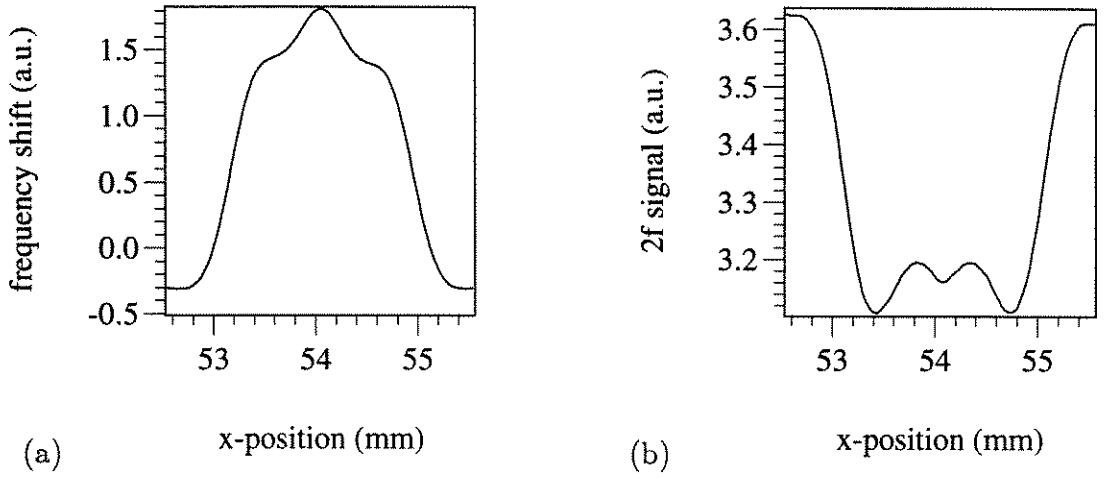

Figure 34: Position dependence of (a) frequency shift and (b) 2f signal for the $La_{0.7}Ca_{0.3}MnO_3$ thin film

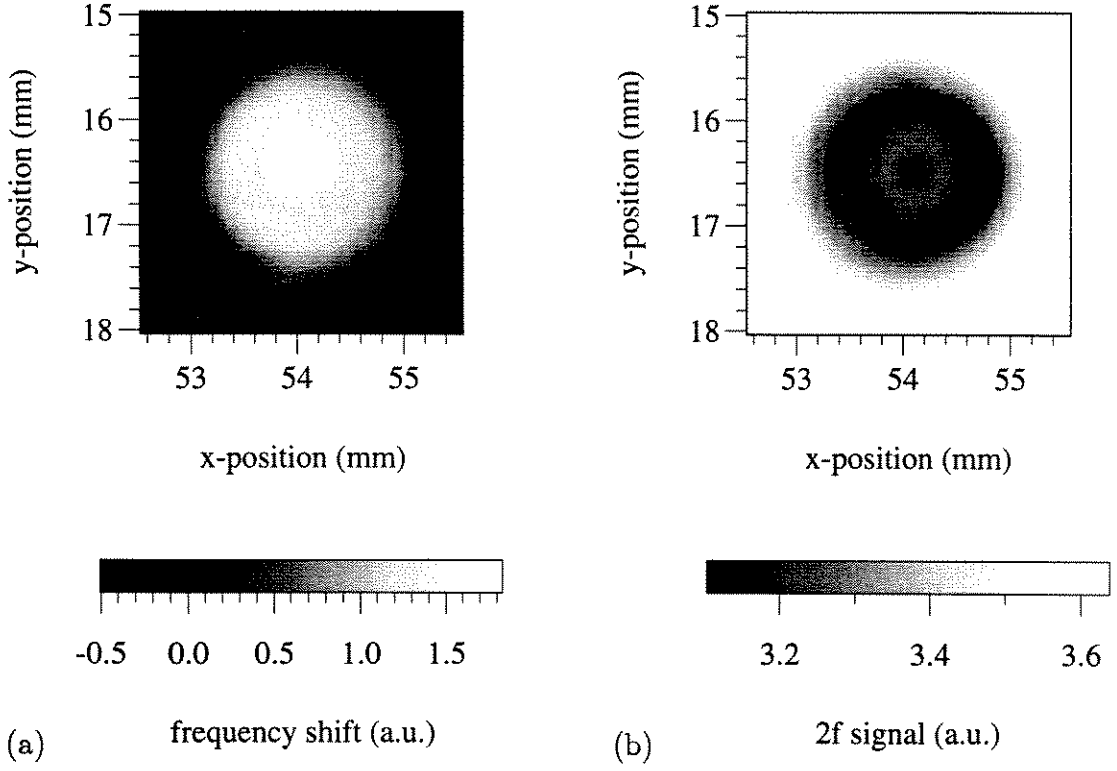

Figure 35: Gray scale plots of (a) frequency shift and (b) 2f signal for the $La_{0.7}Ca_{0.3}MnO_3$ thin film

shortens the resonator less effectively than the gold contact.

Here the frequency shift as well as the 2f signal show features inside the Corbino disk and these are symmetric around the center of the disk. The features in the center of the disk have a size of the order of the spatial resolution of this probe, 500 μm. Therefore it is hard to exactly determine their origin, but the general cylindrical symmetry will have an effect as well as the center gold contact.

These measurements show that at least for the thin film there is a difference whether the probe is directly above the center of the sample or slightly next to the center. However, for several reasons it is hard to draw conclusions that will also apply to our actual Corbino experiment. Firstly, the single crystal did not show those effects, but the single crystal is also harder to measure with the microscope than the thin film. Secondly, the probe of the microscope is held above the sample, whereas in the Corbino geometry we require direct electrical contact. Finally, the diameter of the microscope probe is not exactly the diameter of the Corbino sample.

Thus the thin film data suggests that the alignment of the Corbino probe with respect to the sample disk has influence on the actually measured surface impedance, but the effect in case of the single crystal is hard to estimate.

References

[1] R. von Helmolt, J. Wecker, B. Holzapfel, L. Schultz, and K. Samwer, Phys. Rev. Lett. **71**, 2331 (1993); S. Jin, T.H. Tiefel, M. McCormack, R.A. Fastnacht, R. Ramesh, and L.H. Chen, Science **264**, 413 (1994)

[2] For a review of CMR: A.P. Ramirez, J. Phys. Condens. Matter **9**, 8171 (1997)

[3] J.C. Booth, "Novel Measurements of the Frequency Dependent Microwave Surface Impedance of Cuprate Thin Film Superconductors", Ph. D. Thesis, University of Maryland, 1996

[4] J.C. Booth, D.H. Wu, and S.M. Anlage, Rev. Sci. Instrum. **65**. 2082 (1994)

[5] D.H. Wu, J.C. Booth, and S.M. Anlage, Phys. Rev. Lett. **75**, 525 (1995); J.C. Booth, D.H. Wu, S.B. Qadri, E.F. Skelton, M.S. Osofsky, A. Pique, and S.M. Anlage, Phys. Rev. Lett. **77**, 4438 (1996)

[6] The error model described here and used by the NWA can be found in Hewlett-Packard Company, "Student Guide for Basic Network Measurements Using the HP8510 Network Analyzer System", edition 4.0, 1991

[7] B. Lax, K. J. Button, "Microwave Ferrites and Ferrimagnetics", New York, 1962

[8] P.J.B. Clarricoats, "Microwave Ferrites", New York, 1961; S.M. Bhagat "Ferromagnetic Resonance", ASTM Metals Handbook, 9th edition **10**, 267 (1986); E. Kneller, "Ferromagnetismus", Berlin, 1962

[9] V.V. Srinivasu, S.E. Lofland, and S.M. Bhagat, J. Appl. Phys. **83**, 2866 (1998)

[10] Here the temperature dependence magnetization is assumed to follow the form $M(T) = 0.08 \cdot (305 - T)^{0.45}$. The resistivity is a third order polynomial fit of

the dc resistance measured during our experiments, that was scaled at the lowest and highest temperatures to the resisitivity given in [13], to eliminate the effect of the offset due to the two point measurement.

[11] A. Urushibara, Y. Moritomo, T. Arima, A. Asamitsu, G. Kido, Y. Tokura, Phys. Rev. B **51**, 14103 (1995)

[12] A.M. Balbashov, S.G. Karabashev, Ya.M. Mukovskiy, and S.A. Zverkov, J. Cryst. Growth **167**, 365 (1996)

[13] S.E. Lofland, S.M. Bhagat, K. Ghosh, R.L. Greene, S.G. Karabashev, D.A. Shulyatev, A.A. Arsenov, and Y. Mukovskii, Phys. Rev. B **56**, 13705 (1997)

[14] A general introduction of critical behavior can be found for example in R.K. Pathria, Statistical Mechanics, 2nd edition, Oxford 1996

[15] K. Ghosh, C.J. Lobb, R.L. Greene, S.G. Karabashev, D.A. Shulyatev, A.A. Arsenov, and Y. Mukovskii, Phys. Rev. Lett. **81**, 4740 (1998); S.E. Lofland, V. Ray, P.H. Kim, S.M. Bhagat, M.A. Manheimer, and S.D. Tyagi, Phys. Rev. B **55**, 2749 (1997); R.H. Heffner, L.P. Le, M.F. Hundley, J.J. Neumeier, G.M. Luke, K. Kolima, B. Nachumi, Y.J. Uemura, D.E. MacLaughlin, and S-W.Cheong, Phys. Rev. Lett. **77**, 1869 (1996)

[16] Ch.V. Mohan, M. Seeger, H. Kronmüller, P. Muragaraj, and J. Maier, J. Magn. Magn. Mat. **183**, 348 (1998)

[17] M. Dominguez, S.E. Lofland, S.M. Bhagat, A.K. Raychaudhuri, H.L. Ju, T. Venkatesan, and R.L. Greene, Solid State Commun. **97**, 193 (1996)

[18] C.P. Vlahacos, R.C. Black, S.M. Anlage, A.Amar, and F.C. Wellstood, Appl. Phys. Lett. **69**, 3272 (1996); D.E. Steinhauer, C.P.Vlahacos, S.K. Dutta, B.F. Feenstra, F.C. Wellstood, and S.M. Anlage, Appl. Phys. Lett. **72**, 861 (1998)